

P-73

NASA
Contractor Report 179620

AVSCOM
Technical Report 87-C-16

LEWIS
GRANT
N-31

79447

A Simplified Computer Solution for the Flexibility Matrix of Contacting Teeth for Spiral Bevel Gears

(NASA-CR-179620) A SIMPLIFIED COMPUTER
SOLUTION FOR THE FLEXIBILITY MATRIX OF
CONTACTING TEETH FOR SPIRAL BEVEL GEARS
Final Report (Northwestern Univ.) 73 p
Avail: NTIS AD-A04/MF A01

N87-23977

Unclass
0079447

C.Y. Hsu and H.S. Cheng
Northwestern University
Evanston, Illinois

June 1987

Prepared for
Lewis Research Center
Under Grant NAG-3143



National Aeronautics and
Space Administration



TABLE OF CONTENTS

	Page
CHAPTER	
I	INTRODUCTION.....1
II	ELASTIC COEFFICIENTS.....2
	2.1 Deflection of Tooth Fixed on Root Cone.....2
	2.2 Deflection of Wheel and Shaft.....3
	2.2.1 Deflections Due to Bending Moment.....4
	2.2.2 Deflections Due to Shearing Strain.....11
	2.2.3 Deflections Due to Axial Force.....16
	2.2.4 Deflections Due to Torsion..... 18
III	DISCUSSION OF RESULTS.....32
	3.1 Comparison with Charles Chao's Results.....32
	3.2 Effect of Mass and Moment of Inertia.....33
	3.3 Effect of Stiffness.....33
	3.4 Effect of Damping Coefficient.....34
IV	CONCLUSIONS.....41
REFERENCES.....	43
NOMENCLATURE.....	45
APPENDIX A - TWO SAMPLES OF INPUT DATA FOR SAPIV	48
APPENDIX B - DEFLECTION AND SLOPE AT POINT B	66

CHAPTER I

INTRODUCTION

In order to calculate the dynamic loads between contacting teeth of spiral bevel gears, it is necessary to compute first the elastic deformation of the tooth contacting surface under an unit normal load located at any arbitrary point on the surface. This was accomplished by Chao(1) using the finite element method. To insure accuracy, the finite element method was employed not only for the gear tooth but also for the gear wheel, hub and shaft. Such an approach necessitates the use of a large number of elements, and the computer cost was found to be prohibitive.

A simplified method is developed in this report to obtain the flexibility matrix, i.e., the deflection along the direction normal to the surface at each grid point on the tooth face due to an unit normal force acting on this point. In this analysis, an existing finite element code SAPIV was used to compute the deformation of the tooth itself. For the deformation of the gear wheel and shaft, conventional beam theory is employed. The total deformation is obtained by using the principle of superposition.

CHAPTER II

ELASTIC COEFFICIENTS

In order to obtain the deflection in the normal direction due to an unit normal force acting on a given grid point(Fig. 2-1), one can separate the gear into two parts: (1) tooth (2) wheel and shaft(Fig. 2-2). After obtaining the deflections from the above two parts, one can superimpose them to obtain the total deflection. Then the deflection in the normal direction at each grid point on the tooth face can be determined.

2.1 Deflection of Tooth Fixed on Root Cone

By fixing the root of the tooth, the finite element program SAPIV can be used to calculate the displacements of each grid point on the tooth surface for an unit normal load applied at any arbitrary grid point. In this calculation, three dimensional solid elements(eight node brick) are used. Fig. 2-3 shows the node number of a typical spiral bevel tooth which has a profile geometry indentical to that used by Chao(1). Appendix A gives two samples of input data for SAPIV.

2.2 Deflection of Wheel and Shaft

Let us consider the wheel and shaft as a beam. There are two axial planes perpendicular to each other and a transverse plane for the pinion or gear shaft as shown in Fig. 2-4(p. 25) for calculating the displacements in the xy plane. The boundary conditions are (see Fig. 2-5):

$$(D_y)_C = (D_y)_D = 0$$

$$(D_x)_C = 0 \quad (2.1)$$

$$(\theta_x)_E = 0$$

where $(D_y)_C$ is the displacement of point C along the y axis and $(\theta_x)_E$ is the angular displacement about the x axis at point E.

The unit normal force acting at any grid point G (Fig. 2-6) can be replaced by a set of forces and couples applied at the center of the cross section cut by the transverse plane (Fig. 2-4) through the grid point. The principle of superposition is applied here, and the deflection due to the force or the couple can be computed separately as shown in the following sections. These deflections can then be added algebraically to obtain the total deflection.

2.2.1 Deflections Due To Bending Moment

Fig. 2-7 is the free body diagram the unit normal force acting at a grid point on the gear contacting surface has been replaced by a set of forces and couples applied on the center of the cross section cut by the transverse plane through the grid point at a distance L from the y axis.

To obtain the deflection and slope at L , the beam is divided into 3 portions.

(1) $b \leq x < d$

Considering the force equilibrium of the portion of the beam between B and E (Fig. 2-8), one obtains

$$M_2 = P(b - L) - M_0 \quad (2.2)$$

The moment of inertia of the cross sectional area with respect to the neutral axis is

$$I_1 = \frac{\pi(r_s^4 - r_i^4)}{4} \quad (2.3)$$

To obtain the deflection and slope at B due to the force P and moment M_2 , one can consider the deflection owing to P or M_2 separately. Referring to beam deflection table (2) and using the principle of superposition the

following results are obtained

$$y_B = \frac{b - c}{6EI_1} [2P(c - b)(d - b) + M_2(2d - 3b + c)] \quad (2.4)$$

$$y_B' = \frac{1}{6EI_1} [P(c - b)(2d - 3b + c) + 2M_2(d + 2c - 3b)] \quad (2.5)$$

where E is the modulus of elasticity.

Appendix B shows a detailed derivation of the deflection and slope at point B by solving differential equation of the elastic line B C D E.

(2) $a < L < x < b$

Fig 2-9 is the free body diagram for the forces acting on the portion of the beam to the right of point L. One obtains

$$M_3 = P(x - L) - M_0 \quad (2.6)$$

Radius of pitch cone on the cross section passed by the transverse plane at a distance x from the y axis is

$$r_p = x \tan \theta_p \quad (2.7)$$

where θ_p is the pitch angle.

The moment of inertia of the cross-sectional area with respect to the neutral axis at a distance x from the y axis is

$$I_3 = \frac{\pi(x^4 \tan^4 \theta_p - r_i^4)}{4} \quad (2.8)$$

The differential equation is

$$\begin{aligned} y'' &= -\frac{M_3}{EI_3} \\ &= \frac{-4P}{\pi E \tan^4 \theta_p} \left[\frac{x - (L + \frac{M_0}{P})}{x^4 - \frac{r_i^4}{\tan^4 \theta_p}} \right] \end{aligned} \quad (2.9)$$

Let

$$A_5 = \frac{-4P}{\pi E \tan^4 \theta_p} \quad (2.10)$$

$$A_6 = L + \frac{M_0}{P} \quad (2.11)$$

$$A_7 = \frac{r_i}{\tan^4 \theta_p} \quad (2.12)$$

If $r_i \neq 0$

$$y' = A_5 \int \left(\frac{\frac{x - A_6}{4}}{\frac{x^4}{4} - A_7^4} \right) dx + C_5 \quad (2.13)$$

$$y' = A_5 \int \left(\frac{D_1}{x - A_7} + \frac{D_2}{x + A_7} + \frac{D_3 x + D_4}{x^2 + A_7^2} \right) dx + C_5 \quad (2.14)$$

$$= A_5 [D_1 \ln|x - A_7| + D_2 \ln|x + A_7| + \frac{D_3}{2} \ln(x^2 + A_7^2) + \frac{D_4}{A_7} \tan^{-1} \frac{x}{A_7}] + C_5$$

where

$$D_1 = \frac{1}{4A_7^3} (A_7 - A_6) \quad (2.15)$$

$$D_2 = \frac{1}{4A_7^3} (A_6 + A_7) \quad (2.16)$$

$$D_3 = -\frac{1}{2A_7^2} \quad (2.17)$$

$$D_4 = \frac{A_6}{2A_7^2} \quad (2.18)$$

C_5 can be determined from the condition

$$y' = y'_B \text{ at } x = b$$

One obtains

$$C_5 = y_B - A_5[D_1 \ln|b - A_7| + D_2 \ln|b + A_7| + \dots] \quad (2.19)$$

$$\frac{D_3}{2} \ln(b^2 + A_7^2) + \frac{D_4}{A_7} \tan^{-1} \frac{b}{A_7}$$

Separating variables and integrating one obtains

$$y = A_5[D_1(x - A_7) \ln|x - A_7| - D_1(x - A_7) + \dots] \quad (2.20)$$

$$D_2(x + A_7) \ln|x + A_7| - D_2(x + A_7) +$$

$$\frac{D_3 x}{2} \ln(x^2 + A_7^2) - D_3 x + D_3 A_7 \tan^{-1} \frac{x}{A_7} +$$

$$\frac{D_4 x}{A_7} \tan^{-1} \frac{x}{A_7} - \frac{D_4}{2} \ln\left[\left(\frac{x}{A_7}\right)^2 + 1\right] + C_5 x + C_6$$

At $x = b$, $y = y_B$, one obtains

$$C_6 = y_B - A_5[D_1(b - A_7)[\ln|b - A_7| - 1] + \dots] \quad (2.21)$$

$$D_2(b + A_7)[\ln|b + A_7| - 1] + \frac{D_3 b}{2}[\ln(b^2 + A_7^2) -$$

$$2] + \tan^{-1} \frac{b}{A_7} (D_3 A_7 + \frac{D_4 b}{A_7}) - \frac{D_4}{2} \ln\left[\left(\frac{b}{A_7}\right)^2 + 1\right] -$$

$$C_5 b$$

Setting $x = L$, one obtains the deflection and slope of point L

$$y_L = A_5 \{ D_1 (L - A_7) [\ln|L - A_7| - 1] + \quad (2.22)$$

$$D_2 (L + A_7) [\ln|L + A_7| - 1] + \frac{D_3 L}{2} [\ln(L^2 + A_7^2) -$$

$$2] + \tan^{-1} \frac{L}{A_7} (D_3 A_7 + \frac{D_4 L}{A_7}) - \frac{D_4}{2} \ln[(\frac{L}{A_7})^2 + 1] \} +$$

$$C_5 L + C_6$$

$$y'_L = A_5 [D_1 \ln|L - A_7| + D_2 \ln|L + A_7| + \quad (2.23)$$

$$\frac{D_3}{2} \ln(L^2 + A_7^2) + \frac{D_4}{A_7} \tan^{-1} \frac{L}{A_7}] + C_5$$

If $r_i = 0$

$$y' = A_5 \int \left(\frac{x - A_6}{x^4} \right) dx + C_5'$$

$$= - \frac{A_5}{6x^3} (3x - 2A_6) + C_5' \quad (2.24)$$

$$y = \frac{A_5}{6x^2} (3x - A_6) + C_5' x + C_6' \quad (2.25)$$

By knowing $y' = y'_B$ and $y = y_B$ at $x = b$, one obtains

$$c'_5 = y'_B + \frac{A_5}{6b^3}(3b - 2A_6) \quad (2.26)$$

$$c'_6 = y_B - \frac{A_5}{6b^2}(3b - A_6) - c'_5 b \quad (2.27)$$

Replacing x by L into equations (2.24) and (2.25)

$$y_L = \frac{A_5}{6L^2}(3L - A_6) + c'_5 L + c'_6 \quad (2.28)$$

$$y'_L = - \frac{A_5}{6L^3}(3L - 2A_6) + c'_5 \quad (2.29)$$

(3) $a < x < L$

Setting $x = a$ into equations (2.14) and (2.20) (or (2.24) and (2.25) as $r_i = 0$), one obtains y_A and y'_A .

Then

$$y_L = y_A + (L - a)y'_A \quad (2.30)$$

$$y'_L = y'_A \quad (2.31)$$

The displacement of grid point G can be calculated from the displacement of L by virtue of the fact that

G and L lie in the same transverse plane which is assumed to remain plane after deformation.

Fig. 2-10 shows how the grid point G moves to the final position following the displacement of point L. Here

$$D = |y_L| \quad (2.32)$$

$$\theta = |y_L'| \quad (2.33)$$

Hence, one can obtain the displacement of the grid point G by rotation about point L and translation.

2.2.2 Deflections Due to Shearing Strain

Referring to Fig. 2-7 again, one can divide the beam into 3 portions for derivation.

(1) $b < x < c$

$$I_1 = \frac{\pi(r_s^4 - r_i^4)}{4}$$

The maximum shear stress τ_{\max} is induced on neutral plane. So

$$b_1 = 2(r_s - r_i) \quad (2.34)$$

$$\tau_{\max} = \frac{P}{I_1 b_1} \int_{r_i}^{r_s} y dA$$

$$= \frac{8(r_s^3 - r_i^3)P}{3\pi b_1(r_s^4 - r_i^4)} \quad (2.35)$$

Then the slope of the elastic line becomes

$$\frac{dy}{dx} = \frac{\tau_{\max}}{G} \quad (2.36)$$

where G is the shear modulus.

Integrating

$$y = \frac{\tau_{\max}}{G}x + C_7 \quad (2.37)$$

Using the condition: $y = 0$ at $x = c$, one obtains

$$C_7 = -\frac{\tau_{\max}c}{G} \quad (2.38)$$

Then the deflection of point B becomes

$$y_B = \frac{\tau_{\max}b}{G} + C_7 \quad (2.39)$$

(2) $a < L < x < b$

Referring to Fig. 2-9

$$r_p = x \tan \theta_p$$

$$I_2 = \frac{\pi(x^4 \tan^4 \theta_p - r_i^4)}{4} \quad (2.40)$$

$$b_2 = 2(r_p - r_i) \quad (2.41)$$

$$\begin{aligned} \tau_{\max} &= \frac{P}{I_2 b_2} \int_{r_i}^{r_p} y dA \\ &= \frac{P(r_p^2 + r_p r_i + r_i^2)}{3I_2} \end{aligned} \quad (2.42)$$

$$\begin{aligned} \frac{dy}{dx} &= \frac{\tau_{\max}}{G} \\ &= \frac{4P(r_p^2 + r_p r_i + r_i^2)}{3\pi G(r_p^4 - r_i^4)} \end{aligned} \quad (2.43)$$

$$dx = \frac{dr_p}{\tan \theta_p} \quad (2.44)$$

Let

$$A_8 = \frac{4P}{3\pi G \tan \theta_p} \quad (2.45)$$

$$r_{pB} = b \tan \theta_p \quad (2.46)$$

$$r_{pL} = L \tan \theta_p \quad (2.47)$$

If $r_i \neq 0$

$$y = A_8 \int \left(\frac{r_p^2 + r_i r_p + r_i^2}{r_p^4 - r_i^4} \right) dr_p + C_8$$

$$= A_8 [D_5 \ln|r_p - r_i| + D_6 \ln|r_p + r_i| + \frac{D_7}{2} \ln(r_p^2 + r_i^2)] + C_8 \quad (2.48)$$

where

$$D_5 = \frac{3}{4r_i} \quad (2.49)$$

$$D_6 = -\frac{1}{4r_i} \quad (2.50)$$

$$D_7 = -\frac{1}{2r_i} \quad (2.51)$$

Using the condition: $y = y_B$ at $x = b$, one obtains

$$C_8 = y_B - A_8 [D_5 \ln|r_{pB} - r_i| + D_6 \ln|r_{pB} + r_i| + \frac{D_7}{2} \ln(r_{pB}^2 + r_i^2)] \quad (2.52)$$

Setting $x = L$, one obtains the deflection and slope at point L

$$y_L = A_8 [D_5 \ln|r_{pL} - r_i| + D_6 \ln|r_{pL} + r_i| + \frac{D_7}{2} \ln(r_{pL}^2 + r_i^2)] + C_8 \quad (2.53)$$

$$y'_L = \frac{4P(r_{pL}^2 + r_{pL}r_i + r_i^2)}{3\pi G(r_{pL}^4 - r_i^4)} \quad (2.54)$$

If $r_i = 0$

$$\begin{aligned} y &= A_8 \int \frac{1}{r_p^2} dr_p + C_8 \\ &= - \frac{A_8}{r_p} + C_8 \end{aligned} \quad (2.55)$$

Using the condition: $y = y_B$ at $x = b$, one obtains

$$C_8 = y_B + \frac{A_8}{r_{pB}} \quad (2.56)$$

Setting $x = L$, the deflection and slope at point L become

$$y_L = - \frac{A_8}{r_{pL}} + C_8 \quad (2.57)$$

$$y_L' = \frac{4P}{3\pi G r_{pL}^2} \quad (2.58)$$

(3) $a < x < L$

Setting $x = a$ in equations (2.43) and (2.48) (or (2.55) as $r_i = 0$), one obtains y_A and y_A'

$$y_L = y_A + (L - a)y_A' \quad (2.59)$$

$$y_L' = y_A' \quad (2.60)$$

Using the same method discussed in section 2.2.1, one can obtain the displacement of the grid point G by rotation about point L and translation.

2.2.3 Deflection Due to Axial Force

Referring to Fig. 2-7, one can divide the beam into 3 portions for derivation of axial deflections.

(1) $b < x < c$

The cross-sectional area of the shaft is

$$A_i = \pi(r_s^2 - r_i^2) \quad (2.61)$$

The deflection along the axis of the shaft is

$$\delta_1 = \frac{P_t(c - b)}{\pi E(r_s^2 - r_i^2)} \quad (2.62)$$

(2) $a < L < x < b$

$$r_p = x \tan \theta_p$$

The cross-sectional area of the pitch cone is

$$A_{ii} = \pi(x^2 \tan^2 \theta_p - r_i^2) \quad (2.63)$$

$$\begin{aligned}
 d\delta_2 &= \frac{P_t dx}{A_{ii} E} \\
 &= \frac{P_t dx}{\pi E (x^2 \tan^2 \theta_p - r_i^2)} \\
 \delta_2 &= \frac{P_t}{\pi E \tan^2 \theta_p} \int_L^b \frac{1}{(x^2 - \frac{r_i^2}{\tan^2 \theta_p})} dx
 \end{aligned} \tag{2.64}$$

Let

$$\begin{aligned}
 A_9 &= \frac{P_t}{\pi E \tan^2 \theta_p} \\
 A_7 &= \frac{r_i}{\tan \theta_p}
 \end{aligned} \tag{2.65}$$

If $r_i \neq 0$

$$\begin{aligned}
 \delta_2 &= A_9 \int_L^b \left(\frac{1}{x^2 - A_7^2} \right) dx \\
 &= \frac{A_9}{2A_7} \ln \left| \frac{(b - A_7)(L + A_7)}{(b + A_7)(L - A_7)} \right|
 \end{aligned} \tag{2.66}$$

If $r_i = 0$

$$\begin{aligned}
 \delta_2 &= A_9 \int_L^b \frac{dx}{x^2} \\
 &= A_9 \left(\frac{1}{L} - \frac{1}{b} \right)
 \end{aligned} \tag{2.67}$$

(3) $a < x < L$

If $r_i \neq 0$

$$\begin{aligned}\delta_2 &= A_9 \int_a^b \left(\frac{1}{x^2 - A_7^2} \right) dx \\ &= \frac{A_9}{2A_7} \ln \left| \frac{(b - A_7)(a + A_7)}{(b + A_7)(a - A_7)} \right| \quad (2.68)\end{aligned}$$

If $r_i = 0$

$$\begin{aligned}\delta_2 &= A_9 \int_a^b \frac{dx}{x^2} \\ &= A_9 \left(\frac{1}{a} - \frac{1}{b} \right) \quad (2.69)\end{aligned}$$

The displacement of grid point G due to the axial force is

$$\delta = \delta_1 + \delta_2 \quad (2.70)$$

2.2.4 Deflections Due to Torsion

Again, referring to Fig. 2-7, one can divide the beam into 3 portions for derivations of torsional deflections.

(1) $b < x < e$

The polar moment of inertia of the shaft is

$$J_1 = \frac{\pi(r_s^4 - r_i^4)}{2} \quad (2.71)$$

The total angle of twist of this portion becomes

$$\begin{aligned} \phi_1 &= \frac{T(e - b)}{GJ_1} \\ &= \frac{2(e - b)T}{\pi G(r_s^4 - r_i^4)} \end{aligned} \quad (2.72)$$

(2) $a < L < x < b$

$$r_p = x \tan \theta_p$$

$$J_2 = \frac{\pi(x^4 \tan^4 \theta_p - r_i^4)}{2} \quad (2.73)$$

$$d\phi_2 = \frac{Tdx}{GJ_2}$$

$$\begin{aligned} \phi_2 &= \int_L^b \left[\frac{2T}{\pi G(x^4 \tan^4 \theta_p - r_i^4)} \right] dx \\ &= \frac{2T}{\pi G \tan^4 \theta_p} \int_L^b \left(\frac{1}{x^4 - \frac{r_i^4}{\tan^4 \theta_p}} \right) dx \end{aligned} \quad (2.74)$$

Let

$$A_{10} = \frac{2T}{\pi G \tan^4 \theta_p} \quad (2.75)$$

$$A_7 = \frac{r_i}{\tan \theta_p}$$

If $r_i \neq 0$

The total angle of twist of this portion becomes

$$\begin{aligned} \Phi_2 &= A_{10} \int_L^b \left(\frac{1}{x^4} - \frac{1}{A_7^4} \right) dx \\ &= A_{10} \left[\ln \left(\left| \frac{b - A_7}{L - A_7} \right| \right)^{D_9} \cdot \left| \frac{b + A_7}{L + A_7} \right|^{D_{10}} \right] + \\ &\quad \frac{D_{12}}{A_7} \left(\tan^{-1} \frac{b}{A_7} - \tan^{-1} \frac{L}{A_7} \right) \quad (2.76) \end{aligned}$$

where

$$D_9 = \frac{1}{4A_7^3} \quad (2.77)$$

$$D_{10} = -\frac{1}{4A_7^3} \quad (2.78)$$

$$D_{12} = -\frac{1}{2A_7^2} \quad (2.79)$$

If $r_i = 0$

$$\begin{aligned}\Phi_2 &= A_{10} \int_a^b \frac{dx}{x^4} \\ &= \frac{A_{10}}{3} \left(\frac{1}{L^3} - \frac{1}{b^3} \right)\end{aligned}\quad (2.80)$$

(3) $L < x < a$

If $r_i \neq 0$

$$\begin{aligned}\Phi_2 &= A_{10} \int_a^b \left(\frac{1}{x^4} - A_7^4 \right) dx \\ &= A_{10} \left[\ln \left(\left| \frac{b - A_7}{a - A_7} \right| \right) \cdot \left| \frac{b + A_7}{a + A_7} \right| \right]^{D_9}_{D_{10}} + \\ &\quad \frac{D_{12}}{A_7} \left(\tan^{-1} \frac{b}{A_7} - \tan^{-1} \frac{a}{A_7} \right)\end{aligned}\quad (2.81)$$

If $r_i = 0$

$$\begin{aligned}\Phi_2 &= A_{10} \int_a^b \frac{dx}{x^4} \\ &= \frac{A_{10}}{3} \left(\frac{1}{a^3} - \frac{1}{b^3} \right)\end{aligned}\quad (2.82)$$

Φ_1 and Φ_2 can then be added to obtain the total angular displacement of the grid point G.

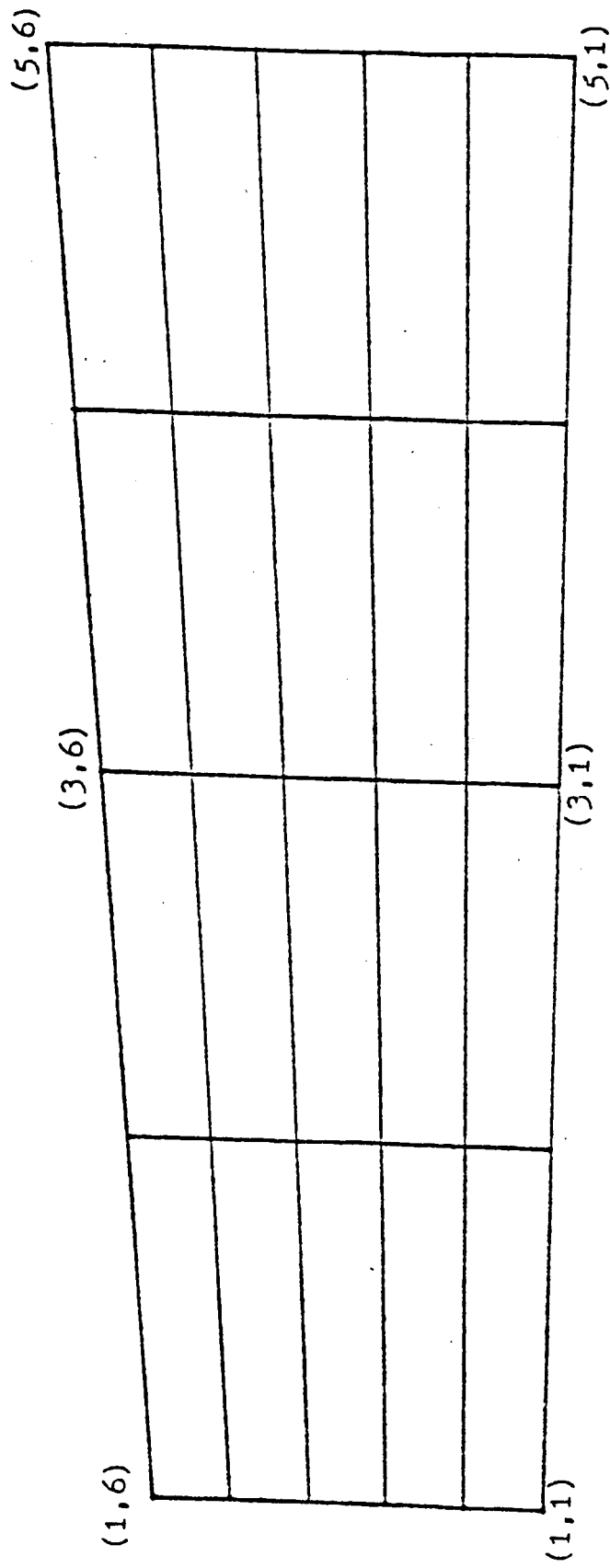


Fig. 2-1 Grid points of a tooth

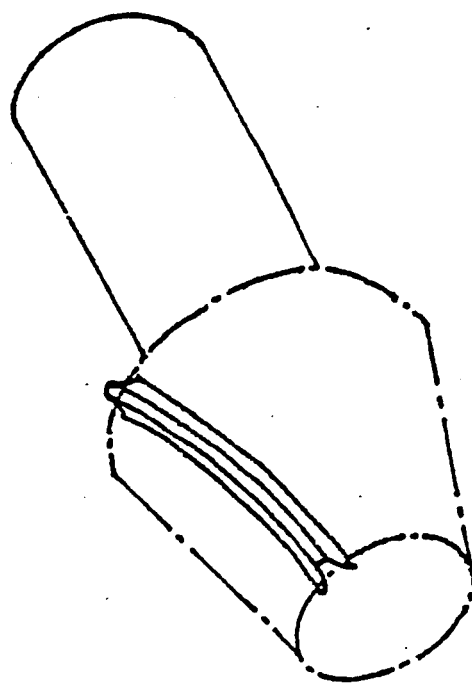
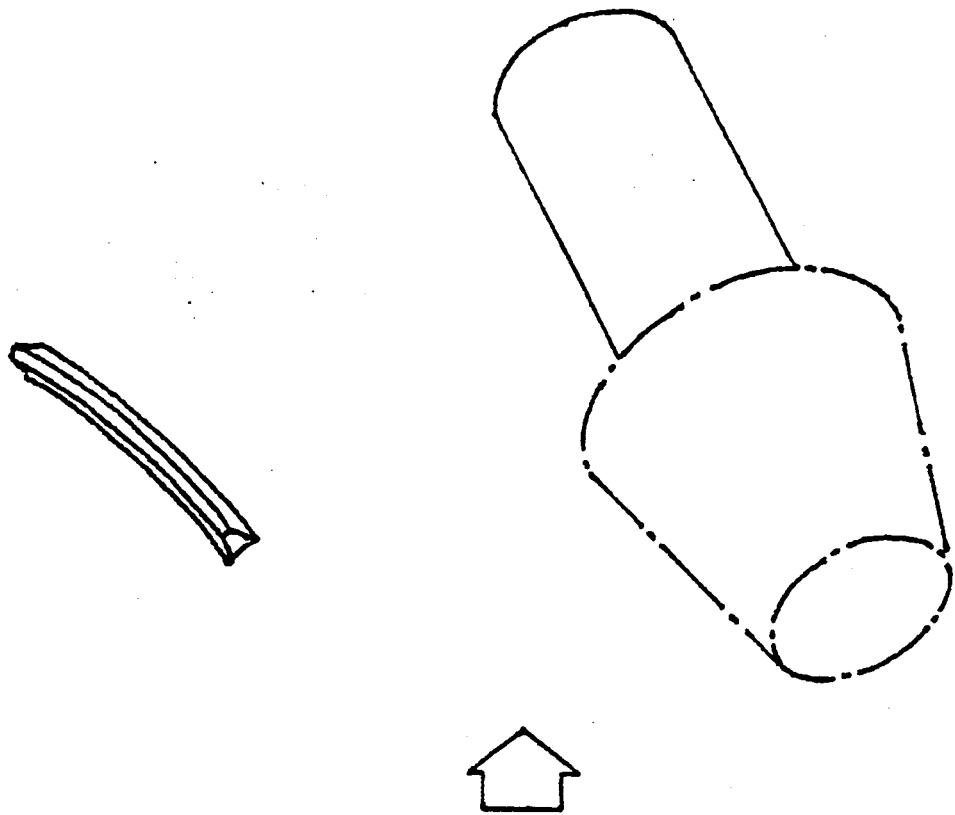


Fig. 2-2 Separation of gear

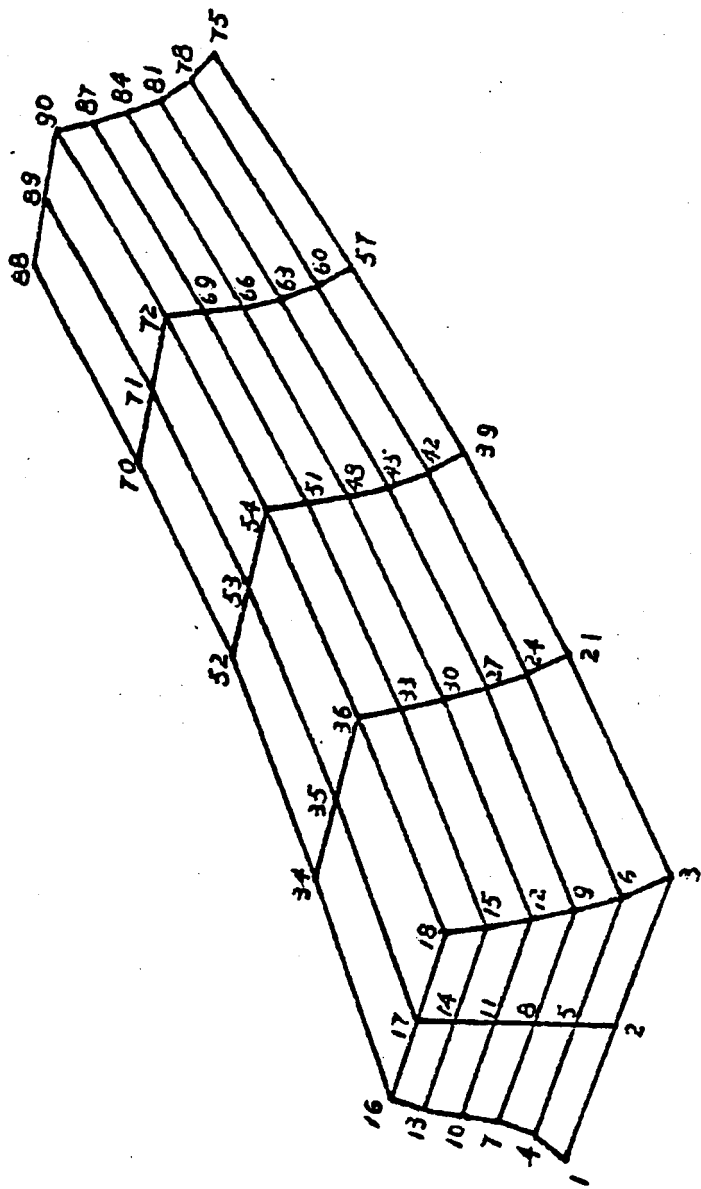


Fig. 2-3 Node number of a tooth

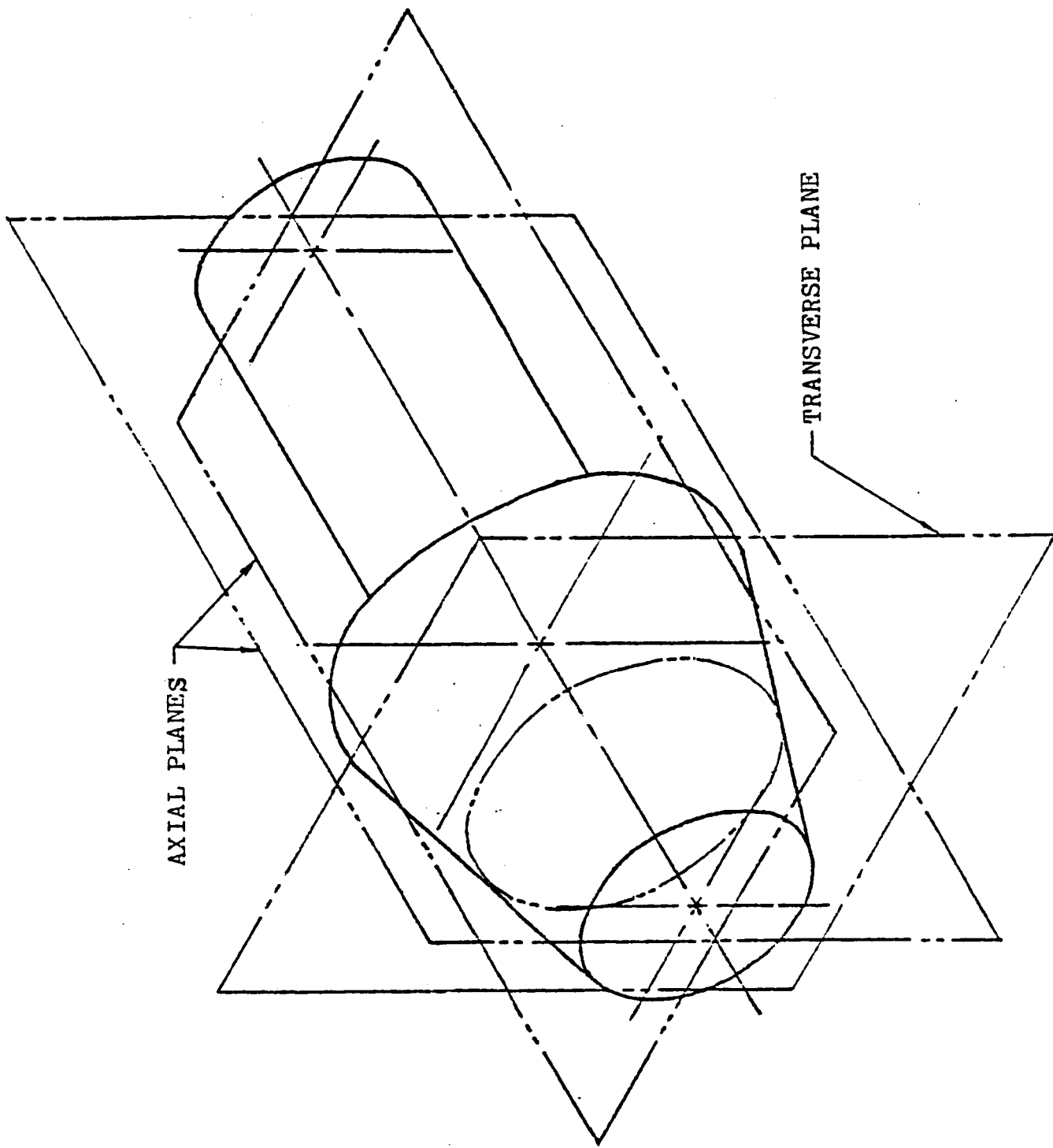


Fig. 2-4 Axial plane and transverse plane

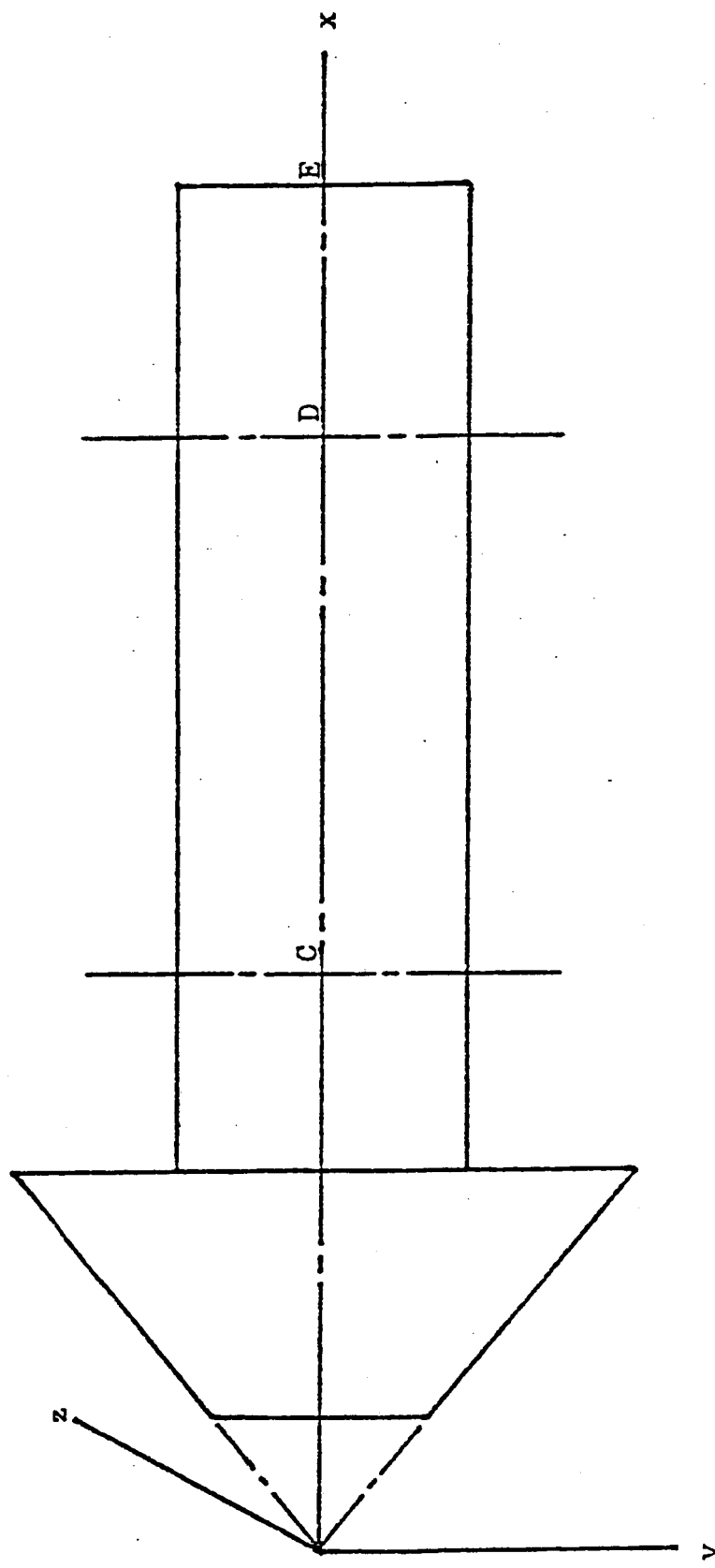


Fig. 2-5 Selection of coordinates for the calculation of deflection of wheel and shaft

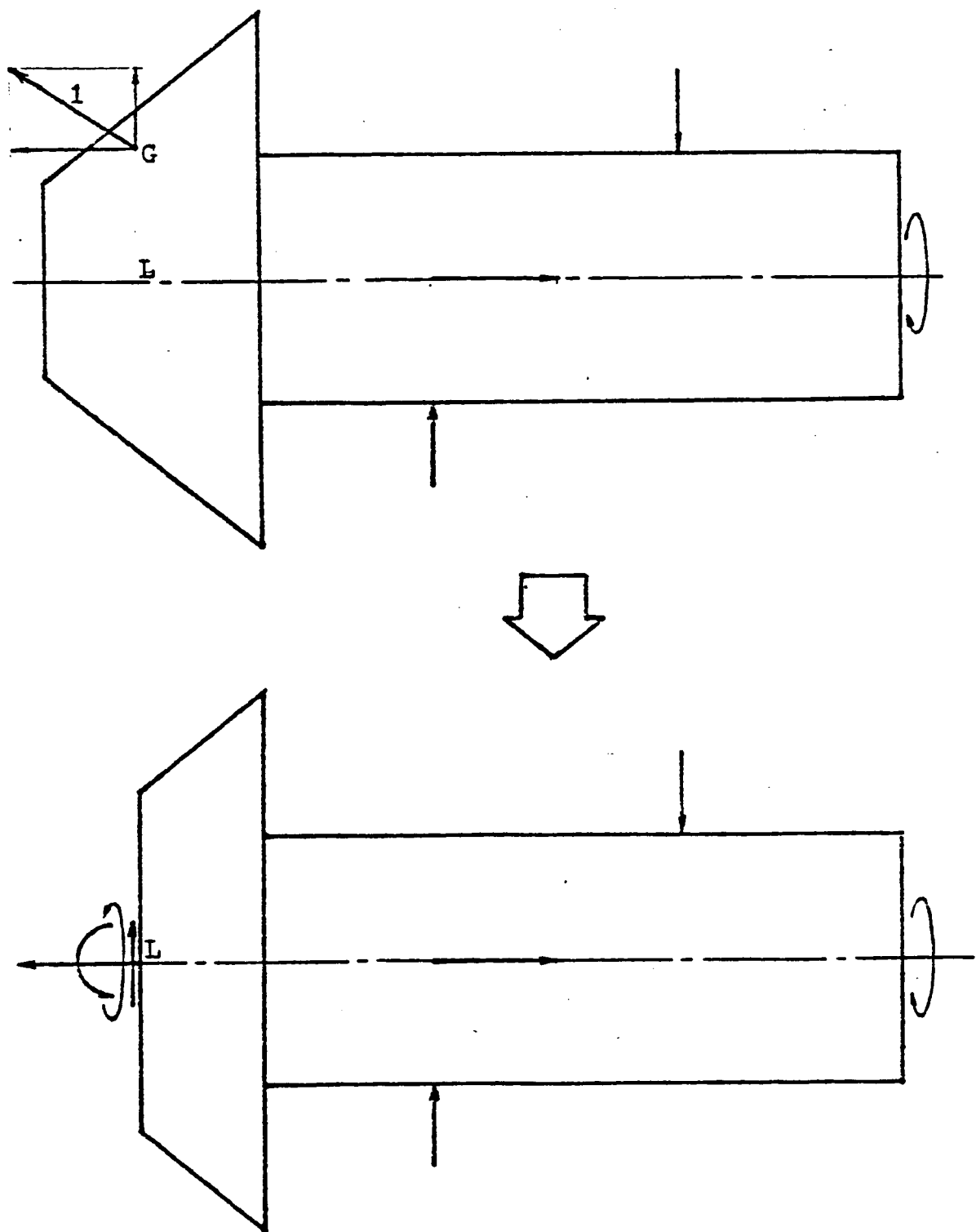


Fig. 2-6 Resolution of the unit normal force
acted on a grid point

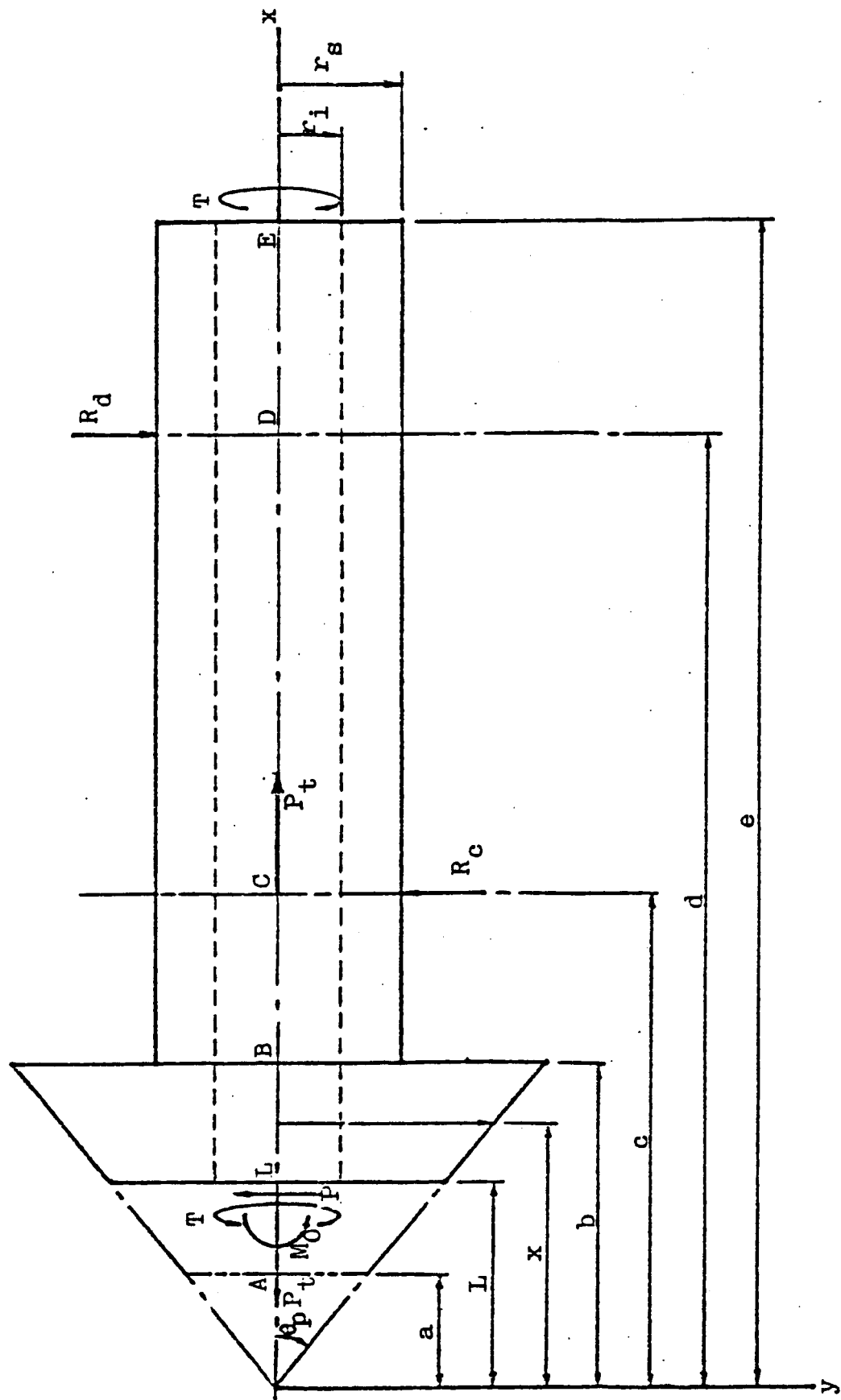


Fig. 2-7 Free body diagram after the resolution of the unit normal force

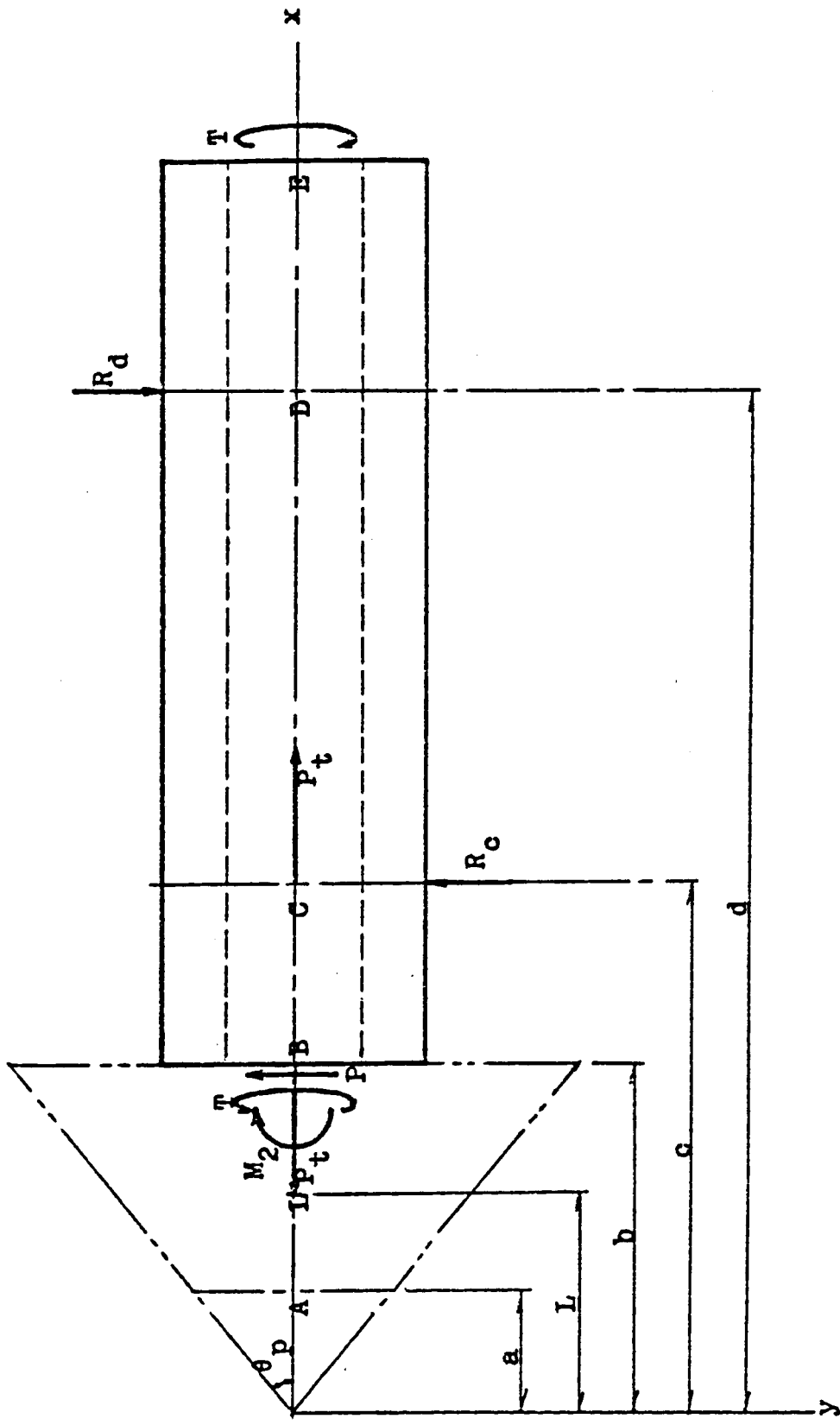


Fig. 2-8 Free body diagram of the beam between the points B and E

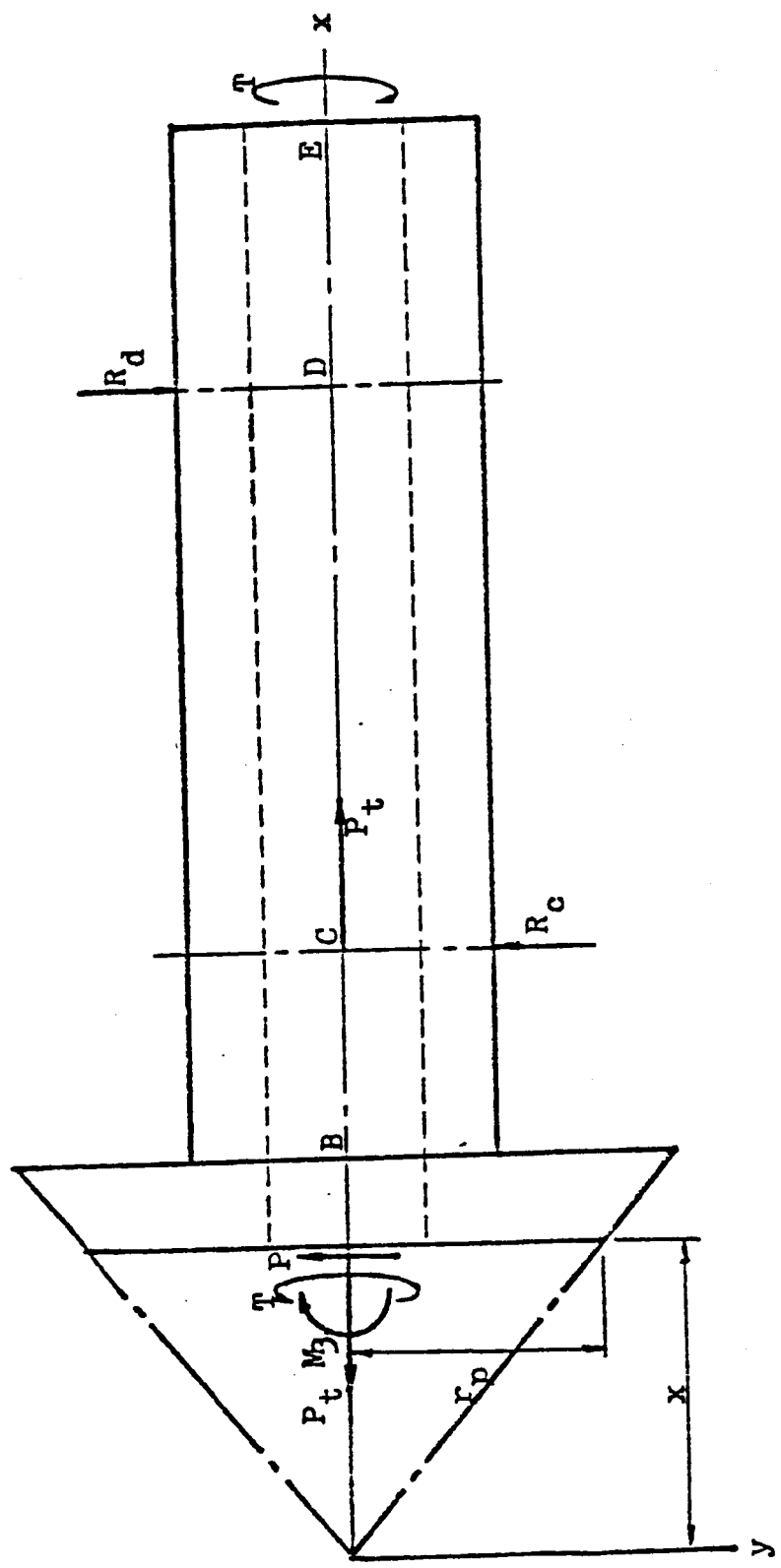


Fig. 2-9 Free body diagram of the beam to the right of point L

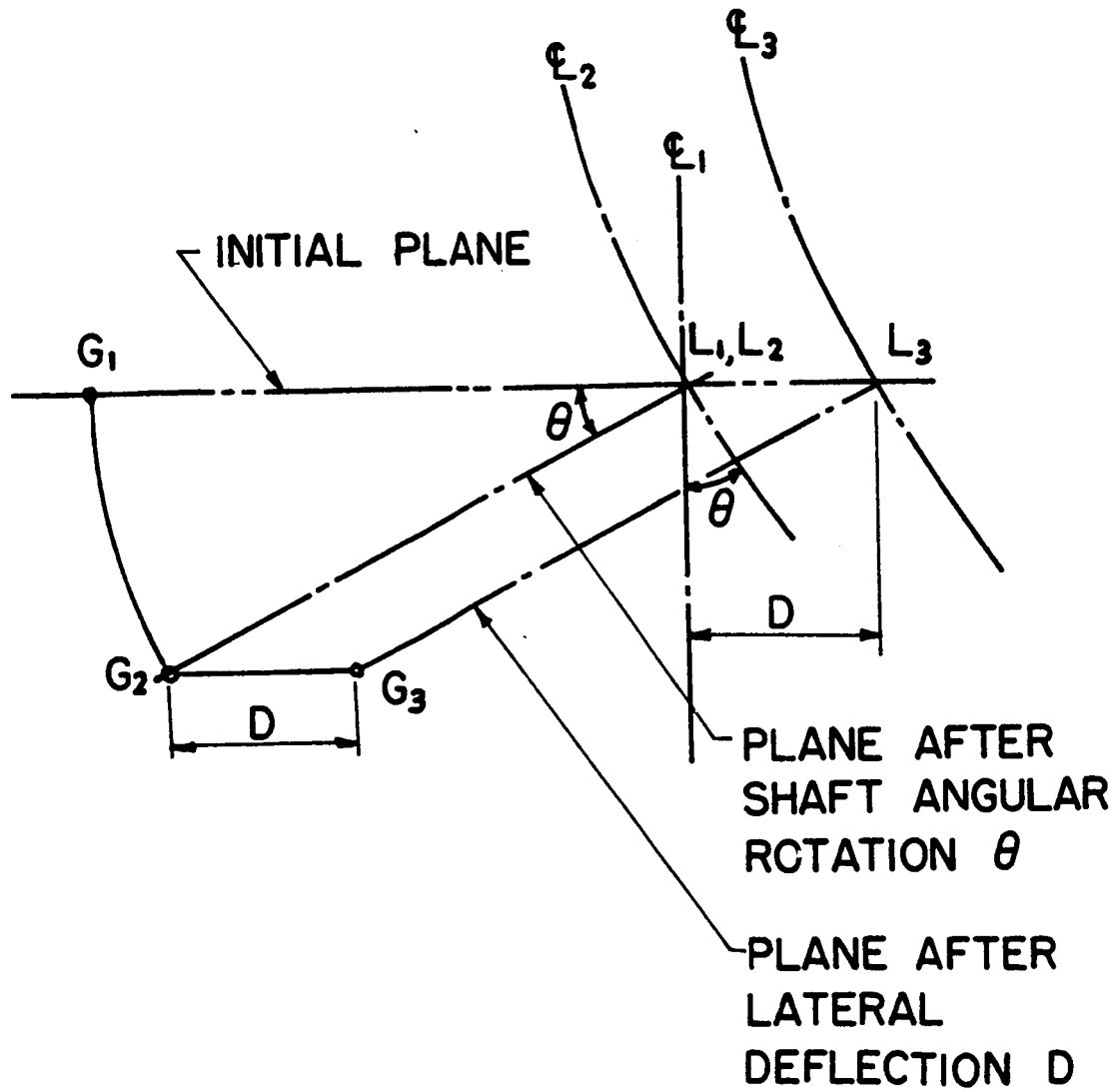


Fig. 2-10. Displacement of the grid point G

CHAPTER III

DISCUSSION OF RESULTS

3.1 Comparison with Charles Chao's Results

Fig. 3-1(p. 35) shows the variation of dynamic load factor (the ratio of the maximum dynamic load along the contact path to the static load at pitch point) as the speed of gear rotation is changed (bearing stiffness = 2,000,000 lbf/in, damping coefficient = 25 lbf.s/in). Since there are 11 degrees of freedom in the spiral bevel gear system, 11 peaks of dynamic load are expected. In the low speed region, a smaller time step in the Runge-Kutta method should be used to facilitate the convergence (Chao used $H = ASTEP/WG$ as the time step in Runge-Kutta method, where ASTEP is the rotational angle of the gear between two adjacent contact points used in Runge-Kutta method and WG is the angular speed of the gear).

Compared with Chao's results in Fig. 3-2, one finds that the peaks in Fig. 3-1 shift toward the left side. The reason is that Chao used smaller masses(m), moments of inertia(I) and flexibility influence coefficients(a) in the gear system. From Dunkerley's Formula(11), one finds

$$\omega_n^2 < \text{tr}(\underline{M}^{-1} \underline{K}) \quad (3.1)$$

where ω_n is the largest resonance frequency, tr means

the trace of the following matrix, \underline{M} is the mass matrix and \underline{K} is the stiffness matrix.

When m and I become larger \underline{M}^{-1} becomes smaller. k (element in the stiffness matrix) is the reciprocal of a . So \underline{K} becomes smaller as a becomes larger. In Fig. 3-1, larger m 's, I 's and a 's are used. Then the upper limit of ω_n^2 becomes smaller. This is why the peaks in Fig. 3-1 shift toward the left side.

3.2 Effect of Mass and Moment of Inertia

The upper bound to the resonance frequencies becomes larger when the mass and moment of inertia become smaller. In Fig. 3-3, all the factors are same as those used in Fig. 3-1, except the m and I are smaller. It is seen that the peaks in Fig. 3-3 shift toward the right.

3.3 Effect of Stiffness

The upper bound to the resonance frequencies becomes larger when the stiffness becomes larger. There are two kinds of stiffness in the spiral bevel gear system - contacting stiffness and bearing stiffness. In Fig. 3-4, a larger contacting stiffness was used in comparison to that used in Fig. 3-1. In contrast, a bearing stiffness smaller than that in Fig. 3-1 was used in Fig. 3-5. Expectedly, the peaks in Fig. 3-4 moves toward right due to stiffer teeth, and the peaks in Fig. 3-5 moves toward left due to a softer bearing stiffness.

3.4 Effect of Damping Coefficient

The change of damping coefficient has little influence on the resonance frequency. But the dynamic load increases as the damping coefficient decreases. In Fig. 3-6, a damping coefficient (DC) 15 lbf.s/in was adopted instead of DC = 25 lbf.s/in in Fig. 3-1. It is clearly see that the dynamic load factor in Fig. 3-6 is considerably increased due to a smaller damping coefficient.

(BS20-DC25)

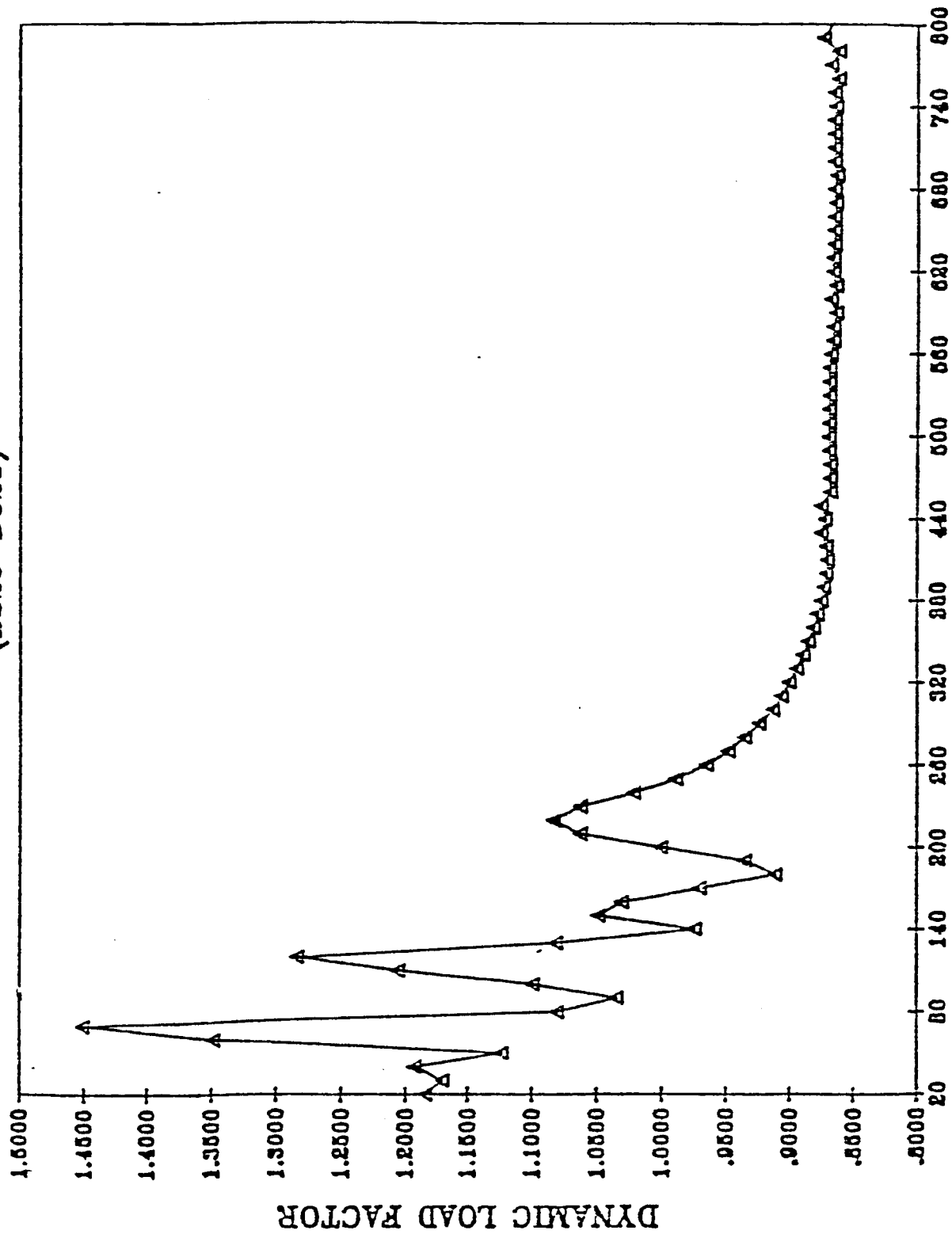


Fig. 3-1 The variation of dynamic load factor as the speed of gear rotation is changed (Hsu's m, I and a, bearing stiffness = 2,000,000 lbf/in, damping coefficient = 25 lbf.s/in)

(DS20-DC25-CMCE)

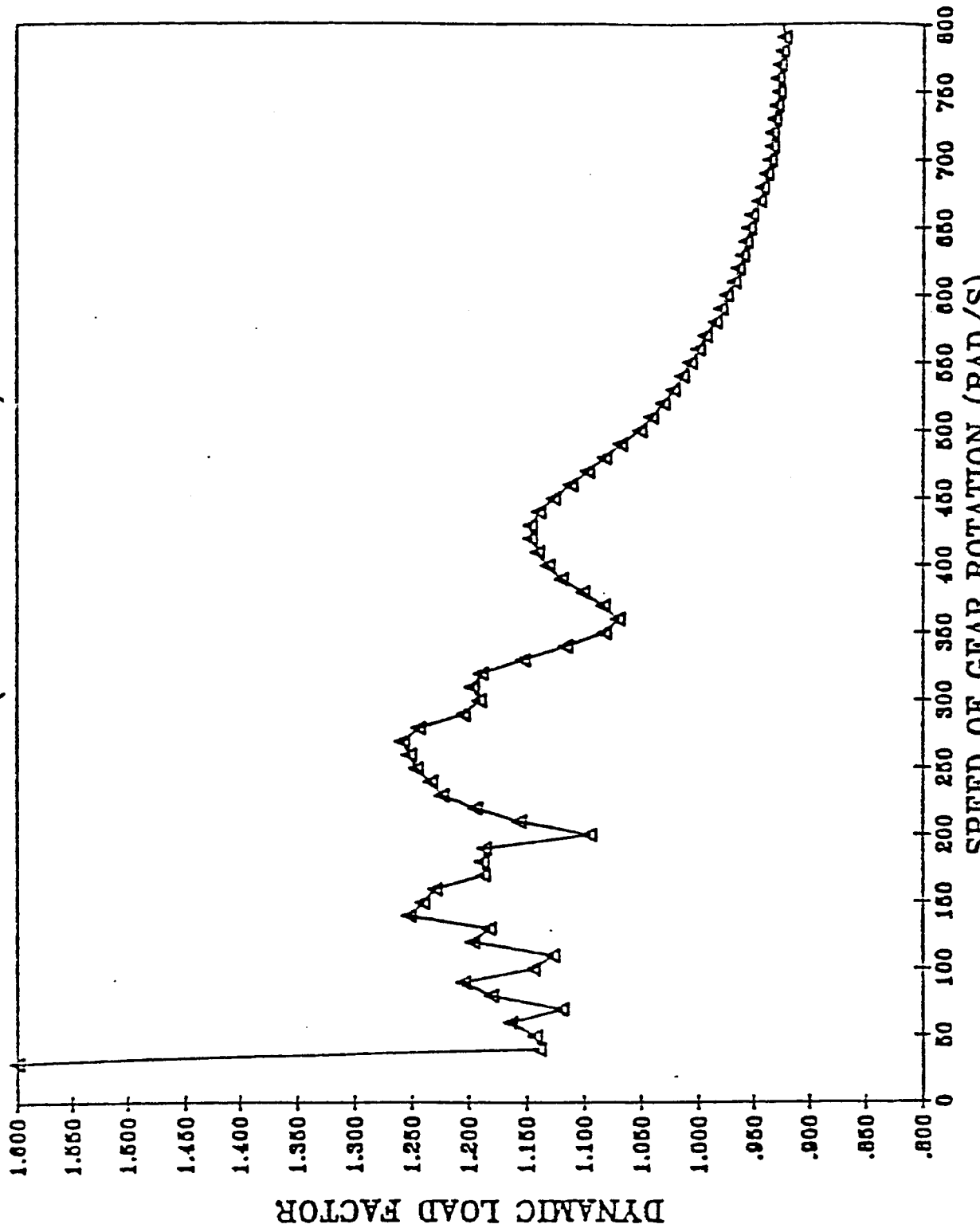


Fig. 3-2 The variation of dynamic load factor as the speed of gear rotation is changed (Chao's m, I and a, bearing stiffness = 2,000,000 lbf/in, damping coefficient = 25 lbf.s/in)

(BS20-DC25-HECM)

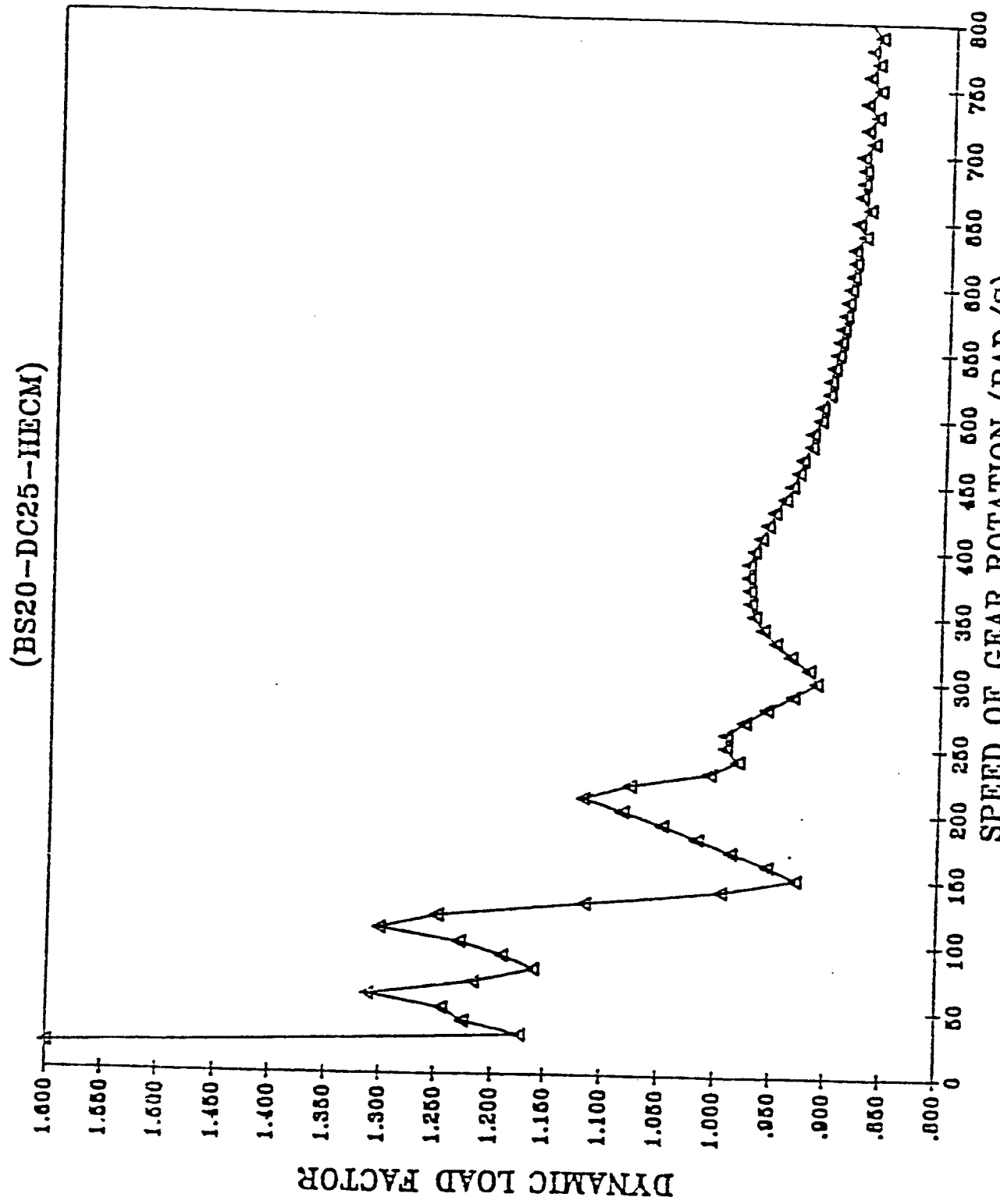


Fig. 3-3. The variation of dynamic load factor as the speed of gear rotation is changed (Chao's m and I, Hsu's a, bearing stiffness = 2,000,000 lbf/in, damping coefficient = 25 lbf.s/in)

(BS20-DC25-HMCE)

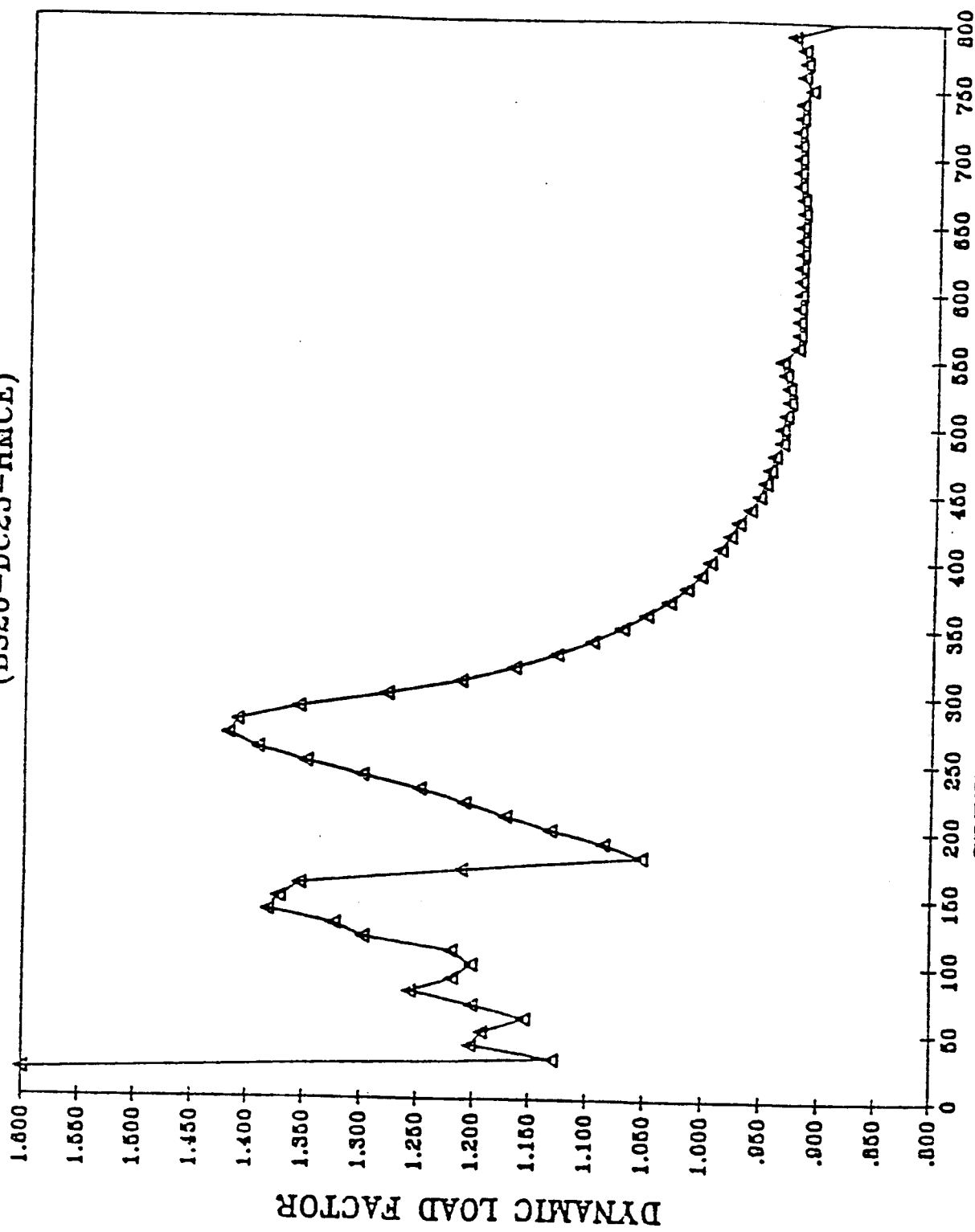


Fig. 3-4 The variation of dynamic load factor as the speed of gear rotation is changed (Hsu's a and I, Chao's a, bearing stiffness = 2,000,000 lbf/in, damping coefficient = 25 lbf.s/in)

(BS10-DC25)

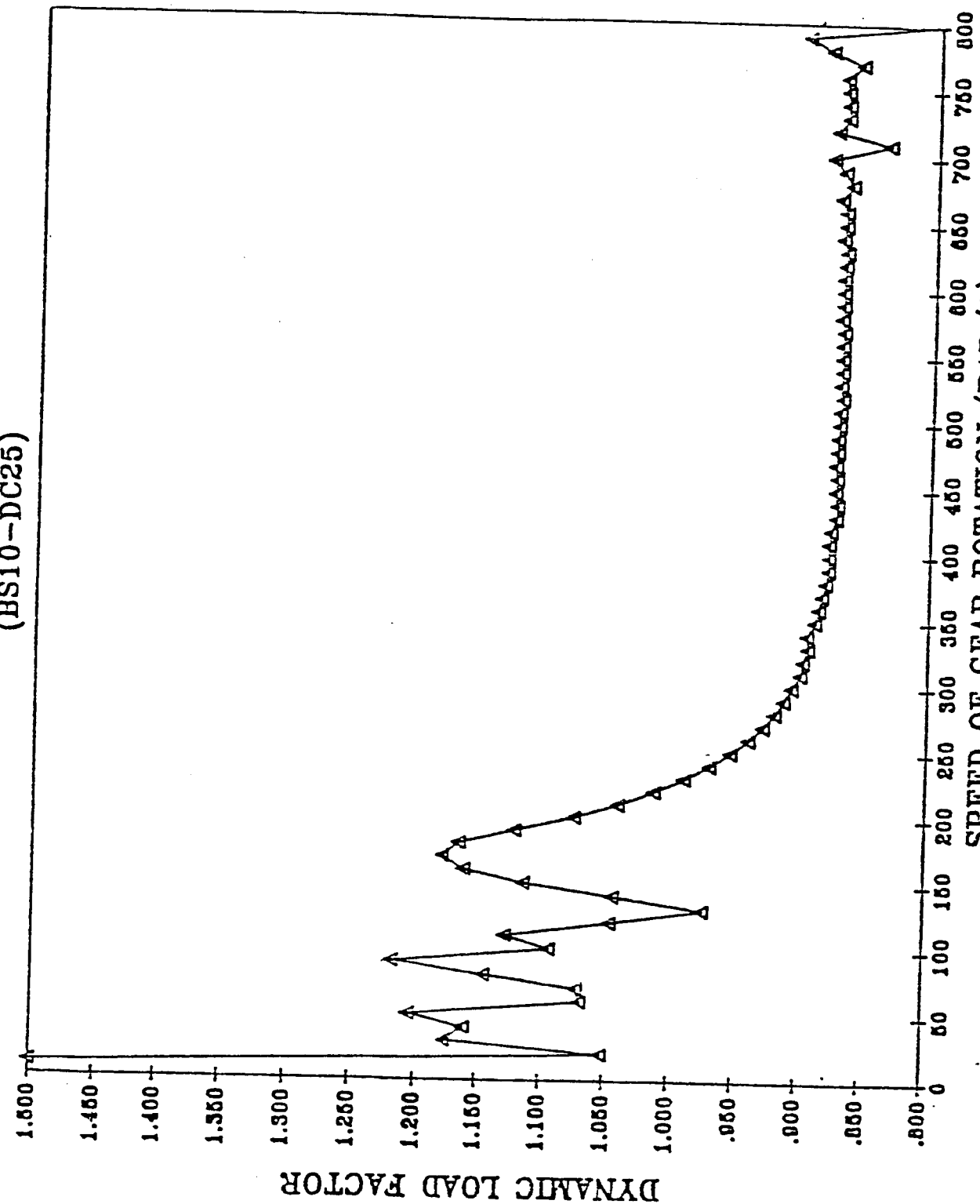


Fig. 3-5 The variation of dynamic load factor as the speed of gear rotation is changed (Hsu's m, I and a, bearing stiffness = 1,000,000 lbf/in, damping coefficient = 25 lbf.s/in)

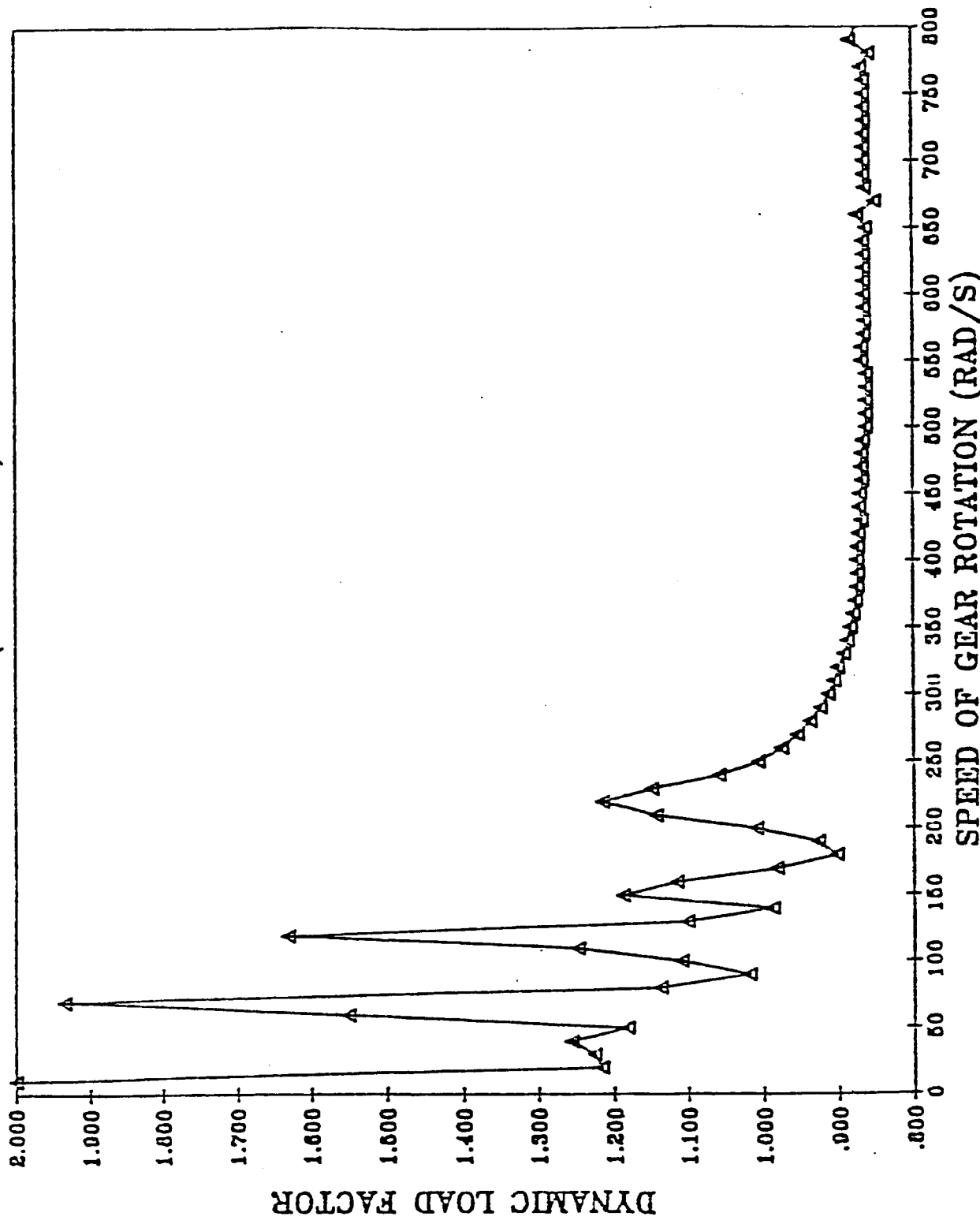


Fig. 3-6 The variation of dynamic load factor as the speed of gear rotation is changed (Iisu's m, I and a, bearing stiffness = 2,000,000 lbf/in, damping coefficient = 15 lbf.s/in)

CHAPTER IV

CONCLUSIONS

A computer code "FLEXM" was developed to calculate the flexibility matrices of contacting teeth for spiral bevel gears using a simplified analysis based on the elementary beam theory for the deformation of gear and shaft. The simplified method requires a computer time at least one order of magnitude less than that needed for the complete FEM (Finite Element Method) Analysis reported earlier by H. C. Chao, and it is much easier to apply for different gear and shaft geometry. Results were obtained for a set of spiral bevel gears whose dimensions are shown in Fig. 4-1. In this case the teeth deflections due to torsion, bending moment, shearing strain and axial force were found to be in the order 10^{-5} , 10^{-6} , 10^{-7} , and 10^{-8} respectively. Thus, for these gears, the torsional deformation is the most predominant part.

In the analysis of dynamic load, resonance frequencies were found to be larger when the mass or moment of inertia is smaller or the stiffness is larger. The change in damping coefficient has little influence on the resonance frequency, but has a marked influence on the dynamic load at the resonant frequencies.

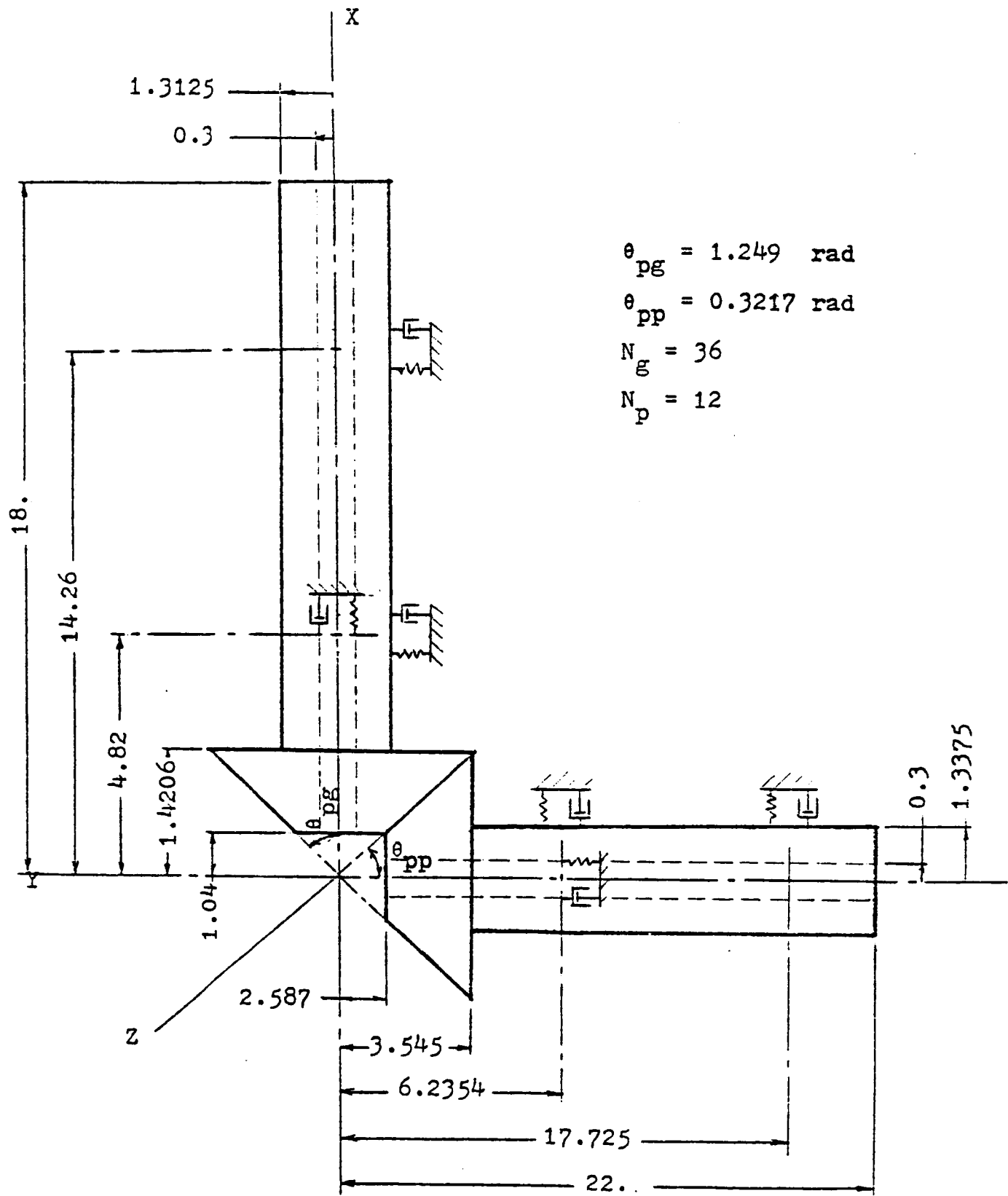


Fig. 4-1 The dimensions for a set of spiral bevel gears

REFERENCES

- (1) Chao, H. C. and Cheng, H. S., "A Computer Solution for the Dynamic Load, Lubricant Film Thickness and Surface Temperatures in Spiral Bevel Gears," NASA CR-4077, 1987.
- (2) Roark, R. J. and Young, W. C., "Formulas for Stress and Strain" McGraw-Hill Book Company, Inc., New York, 1975.
- (3) Chao, H. C., "Tooth Profile and Contact Pattern of Spiral Bevel Gears," M. S. Thesis, Northwestern University, September 1979.
- (4) Chao, H. C., "A Computer Solution for the Dynamic Load, Lubricant Film Thickness and Surface Temperatures in Spiral Bevel Gears," Ph.D. Dissertation, Northwestern University, June 1982.
- (5) Coy, J. J. and Chao, H. C., "A Method of Selecting Grid Size to Account for Hertz Deformation in Finite Element Analysis of Spur Gears," Journal of Mechanical Design, 81-DET-116.
- (6) Wang, K. L. and Cheng, H. S., "A Numerical Solution to the Dynamic Load, Film Thickness, and Surface Temperatures in Spur Gears, Part I Analysis," ASME Trans., Journal of Mechanical Design, Volume 103, January 1981, pp. 177-87.
- (7) Wang, K. L. and Cheng, H. S., "A Numerical Solution to the Dynamic Load, Film Thickness, and Surface Temperatures in Spur Gears, Part II-Results," ASME Trans. Journal of Mechanical Design, Volume 103, January 1981, pp. 188-94.

- (8) Bathe, K. J., Wilson, E. L. and Peterson, F. E. "SAP IV : A Structural Analysis Program for Static and Dynamic Response of Linear System," National Science Foundation Contract Report EERC 73-11.
- (9) Timoshenko, S. P. and Young, D. H., "Elements of Strength of Materials," D. Van Nostrand Company, Inc., Princeton, N. J., 1968.
- (10) Budynas, R. G., "Advanced Strength and Applied Stress Analysis," McGraw-Hill Book Company, Inc., 1977.
- (11) Thomson, W. T., "Theory of Vibration with Applications." Prentice-Hall, Inc., Englewood Cliffs, New Jersey, 1981.
- (12) Spotts, M. F., "Design of Machine Elements" Prentice-Hall, Inc., Englewood Cliffs, New Jersey, 1978.
- (13) "AGMA Standard Gear Nomenclature," American Gear Manufacturers Association, AGMA 112. 04, August, 1965.
- (14) Johnson, R. E. and Kiockemeister, F. L., "Calculus," Allyn and Bacon, Inc., Boston, Mass., 1966.
- (15) Gerald, C. F., "Applied Numerical Analysis," Addison-Wesley Publishing Company, Inc., 1978.

NOMENCLATURE

a(in Chapter II) length along gear (or pinion) axis from the apex of pitch cone to the front plane (refer to Fig. 2-7)

a(in Chapter III) flexibility influence coefficient

b length along gear (or pinion) axis from the apex of pitch cone to the back plane (refer to Fig. 2-7)

c length along gear (or pinion) axis from the apex of pitch cone to the center point of thrust bearing (refer to Fig. 2-7)

DC damping coefficient

$(D_x)_C$ displacement of point C along x axis

d length along gear (or pinion) axis from the apex of pitch cone to the center point of radial bearing (refer to Fig. 2-7)

E modulus of elasticity

e length along gear (or pinion) axis from the apex of pitch cone to the end plane of shaft (refer to Fig. 2-7)

G shear modulus

I moment of inertia

K stiffness matrix

L	length along gear (or pinion) axis from the apex of pitch cone to the transverse plane through the grid point G (refer to Fig. 2-7)
M	moment
<u>M</u>	mass matrix
m	mass
P	shear force
P_t	force along axis of shaft
r_i	radius of hole (refer to Fig. 2-7)
r_p	radius of pitch cone on the cross section passed by transverse plane at a distance x from y axis
r_s	radius of shaft (refer to Fig. 2-7)
T	torque about x axis
y_B	deflection at B in y direction
y'_B	slope at B
δ	deflection along axis of shaft
θ_p	pitch angle
$(\theta_x)_E$	angular displacement about x axis at point E
ϕ	twist angle about x axis

τ_{\max} maximum shear stress

ω_n the largest resonance frequency

APPENDIX A

TWO SAMPLES OF INPUT DATA FOR SAPIV

123456789	123456789	123456789	123456789	123456789	123456789	123456789	123456789	123456789	123456789	123456789	123456789	123456789	123456789	123456789
56789														
250	17													
	70.000													
260	18													
	70.000													
270	19	1	1	1	1	1	1	1.1352225-2.6996818	.3451271					
	70.000													
280	20	1	1	1	1	1	1	1.1352028-2.7170012	.1592737					
	70.000													
290	21	1	1	1	1	1	1	1.1351831-2.7215411	-.0273304					
	70.000													
300	22							1.0803056-2.7208453	.3218651					
	70.000													
310	23							1.0802674-2.7352711	.1589196					
	70.000													
320	24							1.0802293-2.7399470	-.0046002					
	70.000													
330	25							1.0255804-2.7421413	.2973606					
	70.000													
340	26							1.0255730-2.7536389	.1588615					
	70.000													
(S,C OR RETURN)>														
123456789	123456789	123456789	123456789	123456789	123456789	123456789	123456789	123456789	123456789	123456789	123456789	123456789	123456789	123456789
56789														
350	27							1.0255656-2.7581457	.0199593					
	70.000													
360	28							.9708458-2.7631816	.2717251					
	70.000													
370	29							.9708263-2.7719840	.1591097					
	70.000													
380	30							.9708069-2.7761985	.0462282					
	70.000													
390	31							.9158890-2.7839132	.2448944					
	70.000													
400	32							.9159172-2.7901563	.1595966					
	70.000													
410	33							.9159454-2.7937865	.0741464					
	70.000													
420	34							.8611402-2.8046768	.2167437					
	70.000													
430	35							.8611331-2.8084820	.1600917					
	70.000													
440	36							.8611260-2.8111431	.1033747					
	70.000													
(S,C OR RETURN)>														

123456789	123456789	123456789	123456789	123456789	123456789	123456789	123456789	123456789	123456789	123456789	123456789	123456789	123456789	123456789
56739														
450	37	1	1	1	1	1	1	1.2303581-2.9460965	.2087316					
	70.000													
460	38	1	1	1	1	1	1	1.2303544-2.9534790	.0035044					
	70.000													
470	39	1	1	1	1	1	1	1.2303507-2.9465825	-.2017395					
	70.000													
480	40							1.1710455-2.9677205	.1813078					
	70.000													
490	41							1.1710277-2.9732519	.0020571					
	70.000													
500	42							1.1710100-2.9679665	-.1772007					
	70.000													
510	43							1.1116919-2.9891879	.1526480					
	70.000													
520	44							1.1117126-2.9930541	.0010429					
	70.000													
530	45							1.1117332-2.9892363	-.1505618					
	70.000													
540	46							1.0524332-3.0102897	.1228540					
	70.000													
(S,C OR RETURN)>														
123456789	123456789	123456789	123456789	123456789	123456789	123456789	123456789	123456789	123456789	123456789	123456789	123456789	123456789	123456789
56789														
550	47							1.0524284-3.0127978	.0003868					
	70.000													
560	48							1.0524236-3.0103257	-.1220810					
	70.000													
570	49							.9932511-3.0312032	.0917458					
	70.000													
580	50							.9932042-3.0325977	-.0001401					
	70.000													
590	51							.9931573-3.0312075	-.0920260					
	70.000													
600	52							.9338390-3.0518240	.0593035					
	70.000													
610	53							.9338223-3.0523730	-.0005446					
	70.000													
620	54							.9338057-3.0517485	-.0603912					
	70.000													
630	55	1	1	1	1	1	1	1.3255356-3.1849165	.0410155					
	70.000													
640	56	1	1	1	1	1	1	1.3254829-3.1799661	-.1827477					
	70.000													
(S,C OR RETURN)>														

123456789	123456789	123456789	123456789	123456789	123456789	123456789	123456789	123456789	123456789	123456789	123456789
56789											
850	77										
	70.000										
860	78										
	70.000										
870	79										
	70.000										
880	80										
	70.000										
890	81										
	70.000										
900	82										
	70.000										
910	83										
	70.000										
920	84										
	70.000										
930	85										
	70.000										
940	86										
	70.000										
(S,C OR RETURN)>											
123456789	123456789	123456789	123456789	123456789	123456789	123456789	123456789	123456789	123456789	123456789	123456789
56789											
950	87										
	70.000										
960	88										
	70.000										
970	89										
	70.000										
980	90										
	70.000										
990	5	40	1								
1000	1	30000000.		.3		.283		.0000073			
1010		386.									
1020											
1030											
1040											
1050											
1060											
1070	1	1	2	20	19	4	5	23	22	2	1
	70.										
1080	5	13	14	32	31	16	17	35	34	2	1
	70.										
(S,C OR RETURN)>											

123456789 123456789 123456789 123456789 123456789 123456789 123456789 123456789 123456789 123456789 123456789

1350	25	13	.1922	.5016	-.8435
1360	27	14	-.4881	.3509	-.7992
1370	28	15	.2050	.5106	-.8350
1380	30	16	-.5035	.3402	-.7942
1390	31	17	.2178	.5191	-.8265
1400	33	18	-.5170	.3307	-.7895
1410	34	19	.2307	.5273	-.8178
1420	36	20	-.5290	.3222	-.7851
1430	40	21	.1687	.5761	-.7998
1440	42	22	-.4850	.4384	-.7567
1450	43	23	.1796	.5852	-.7908
1460	45	24	-.5024	.4252	-.7529
1470	46	25	.1911	.5940	-.7815
1480	48	26	-.5168	.4139	-.7494
1490	49	27	.2027	.6024	-.7720
1500	51	28	-.5293	.4040	-.7461
1510	52	29	.2143	.6104	-.7626
1520	54	30	-.5405	.3948	-.7429
1530	58	31	.1569	.6570	-.7374
1540	60	32	-.5008	.5096	-.6996

(S,C OR RETURN)>

123456789 123456789 123456789 123456789 123456789 123456789 123456789 123456789 123456789 123456789 123456789

1550	61	33	.1666	.6658	-.7273
1560	63	34	-.5169	.4961	-.6977
1570	64	35	.1769	.6744	-.7169
1580	66	36	-.5301	.4844	-.6959
1590	67	37	.1872	.6826	-.7065
1600	69	38	-.5417	.4740	-.6942
1610	70	39	.1972	.6903	-.6961
1620	72	40	-.5521	.4644	-.6925
1630	76	41	.1449	.7338	-.6637
1640	78	42	-.5168	.5763	-.6331
1650	79	43	.1535	.7424	-.6522
1660	81	44	-.5314	.5627	-.6332
1670	82	45	.1624	.7506	-.6405
1680	84	46	-.5435	.5509	-.6334
1690	85	47	.1713	.7585	-.6288
1700	87	48	-.5540	.5401	-.6335
1710	88	49	.1795	.7660	-.6173
1720	90	50	-.5637	.5300	-.6335

1730

1740

(S,C OR RETURN)>

123456789 123456789 123456789 123456789 123456789 123456789 123456789 123456789 123456789 123456789 123456789 123456789 123456789

56789

1750

1760

1770

1780

1790

1800

1810

1820

1830

1840

1850

1860

1870

1880

1890

1900

1910

1920

1930

1940

(S,C OR RETURN)>

123456789 123456789 123456789 123456789 123456789 123456789 123456789 123456789 123456789 123456789

56789

1950

1960

1970

1980

1990

2000

2010

2020

2030

2040

2050

2060

2070

2080

2090

2100

2110

2120

2130

2140

(S,C OR RETURN)>

123456789 123456789 123456789 123456789 123456789 123456789 123456789 1234
56789

2150
2160
2170
2180
2190
2200
2210
2220
2230
2240
2250
2260 EOI

>

250	17										.9507147-2.5014348	.3277974
	70.000											
260	18										.9404533-2.5014022	.3561410
	70.000											
270	19	1	1	1	1	1					.8276093-2.8262767	-.0357977
	70.000											
280	20	1	1	1	1	1					.8148691-2.8262729	.1444194
	70.000											
290	21	1	1	1	1	1					.7648936-2.8262690	.3186656
	70.000											
300	22										.3821774-2.8076628	-.0104465
	70.000											
310	23										.8690964-2.8076599	.1515968
	70.000											
320	24										.8265055-2.8076571	.3084850
	70.000											
330	25										.9366826-2.7890703	.0148756
	70.000											
340	26										.9233059-2.7890684	.1584728
	70.000											
(S,C OR RETURN)>												
350	27										.8880466-2.7890665	.2983160
	70.000											
360	28										.9903133-2.7705973	.0504391
	70.000											
370	29										.9775167-2.7705719	.1656822
	70.000											
380	30										.9513575-2.7705465	.2786274
	70.000											
390	31										1.0418918-2.7519397	.0948586
	70.000											
400	32										1.0317557-2.7519091	.1726900
	70.000											
410	33										1.0158144-2.7518785	.2495356
	70.000											
420	34										1.0907050-2.7333002	.1470639
	70.000											
430	35										1.0859416-2.7332657	.1791881
	70.000											
440	36										1.0802322-2.7332312	.2111591
	70.000											
(S,C OR RETURN)>												

123456789	123456789	123456789	123456789	123456789	123456789	123456789	123456789	123456789	123456789	123456789	123456789
56789											
650	57	1	1	1	1	1	.9728761-3.3050918	.0498089			
	70.000										
660	58						.9703256-3.2835967	-.3641763			
	70.000										
670	59						1.0208089-3.2835200	-.1791273			
	70.000										
680	60						1.0363269-3.2834433	.0120539			
	70.000										
690	61						1.0410536-3.2620206	-.3557925			
	70.000										
700	62						1.0830462-3.2619149	-.1929779			
	70.000										
710	63						1.0997358-3.2618091	-.0256761			
	70.000										
720	64						1.1142966-3.2402622	-.3357601			
	70.000										
730	65						1.1452837-3.2401834	-.2063931			
	70.000										
740	66						1.1613041-3.2401047	-.0743408			
	70.000										
(S,C OR RETURN)>											
123456789	123456789	123456789	123456789	123456789	123456789	123456789	123456789	123456789	123456789	123456789	123456789
56789											
750	67						.1888861-3.2186494	-.3055537			
	70.000										
760	68						1.2075308-3.2185239	-.2200953			
	70.000										
770	69						1.2200413-3.2183983	-.1335330			
	70.000										
780	70						1.2634673-3.1968262	-.2654222			
	70.000										
790	71						1.2695847-3.1967588	-.2342216			
	70.000										
800	72						1.2749318-3.1966915	-.2028807			
	70.000										
810	73	1	1	1	1	1	.8787037-3.5446358	-.5682845			
	70.000										
820	74	1	1	1	1	1	.9813550-3.5448013	-.3600641			
	70.000										
830	75	1	1	1	1	1	1.0383987-3.5449667	-.1342854			
	70.000										
840	76						.9556396-3.5215521	-.5715815			
	70.000										
(S,C OR RETURN)>											

123456789	123456789	123456789	123456789	123456789	123456789	123456789	123456789	123456789	123456789	123456789	123456789	123456789	123456789	123456789		
56789																
850	77													1.0444118-3.5215666	-.3862172	
	70.000															
860	78													1.0976054-3.5215812	-.1876949	
	70.000															
870	79													1.0325396-3.4984790	-.5748770	
	70.000															
880	80													1.1073122-3.4983428	-.4126808	
	70.000															
890	81													1.1567846-3.4982065	-.2410796	
	70.000															
900	82													1.1142402-3.4751546	-.5663933	
	70.000															
910	83													1.1703313-3.4750532	-.4387410	
	70.000															
920	84													1.2118531-3.4749518	-.3056425	
	70.000															
930	85													1.1990483-3.4518771	-.5473019	
	70.000															
940	86													1.2332332-3.4517915	-.4650465	
	70.000															
(S,C OR RETURN)>																
123456789	123456789	123456789	123456789	123456789	123456789	123456789	123456789	123456789	123456789	123456789	123456789	123456789	123456789	123456789		
56789																
950	87													1.2617830-3.4517060	-.3806732	
	70.000															
960	88													1.2857970-3.4286330	-.5179480	
	70.000															
970	89													1.2959437-3.4285464	-.4918856	
	70.000															
980	90													1.3055622-3.4284599	-.4656248	
	70.000															
990	5	40	1													
1000	1	30000000.												.3	.283	.0000073
1010		386.														
1020																
1030																
1040																
1050																
1060																
1070	1	1	2	20	19	4	5	23	22	2	1	3				
	70.															
1080	5	13	14	32	31	16	17	35	34	2	1					
	70.															
(S,C OR RETURN)>																

123456789 123456789 123456789 123456789 123456789 123456789 123456789 123456789 123456789 123456789 123456789 123456789

56789

1090	6	19	20	38	37	22	23	41	40	2	1	3
	70.											
1100	10	31	32	50	49	34	35	53	52	2	1	
	70.											
1110	11	37	38	56	55	40	41	59	58	2	1	3
	70.											
1120	15	49	50	68	67	52	53	71	70	2	1	
	70.											
1130	16	55	56	74	73	58	59	77	76	2	1	3
	70.											
1140	20	67	68	86	85	70	71	89	88	2	1	
	70.											
1150	21	2	3	21	20	5	6	24	23	2	1	3
	70.											
1160	25	14	15	33	32	17	18	36	35	2	1	
	70.											
1170	26	20	21	39	38	23	24	42	41	2	1	3
	70.											
1180	30	32	33	51	50	35	36	54	53	2	1	
	70.											

(S,C OR RETURN)>

123456789 123456789 123456789 123456789 123456789 123456789 123456789 123456789 123456789 123456789 123456789

56789

1190	31	38	39	57	56	41	42	60	59	2	1	3
	70.											
1200	35	50	51	69	68	53	54	72	71	2	1	
	70.											
1210	36	56	57	75	74	59	60	78	77	2	1	3
	70.											
1220	40	68	69	87	86	71	72	90	89	2	1	
	70.											
1230	4	1	.2459		.5216		-.8170					
1240	6	2	-.6033		-.7862		.1338					
1250	7	3	.3740		.5638		-.7364					
1260	9	4	-.5703		-.8077		.1497					
1270	10	5	.4556		.5940		-.6631					
1280	12	6	-.2475		.2416		-.9383					
1290	13	7	.5149		.6190		-.5930					
1300	15	8	-.3479		.2139		-.9128					
1310	16	9	.5594		.6410		-.5256					
1320	18	10	-.4396		.1876		-.8784					
1330	22	11	.1002		.5567		-.8246					
1340	24	12	-.6334		-.7652		.1154					

(S,C OR RETURN)>

123456789 123456789 123456789 123456789 123456789 123456789 123456789 123456789 123456789 123456789

1350	25	13	.2328	.5959	-.7686
1360	27	14	-.6025	-.7875	.1297
1370	28	15	.3222	.6243	-.7117
1380	30	16	-.4116	.2801	-.8672
1390	31	17	.3899	.6477	-.6546
1400	33	18	-.5045	.2536	-.8253
1410	34	19	.4433	.6682	-.5975
1420	36	20	-.5874	.2286	-.7763
1430	40	21	-.0425	.5924	-.8045
1440	42	22	-.3572	.3740	-.8559
1450	43	23	.0905	.6285	-.7725
1460	45	24	-.4680	.3453	-.8134
1470	46	25	.1845	.6548	-.7329
1480	48	26	-.5621	.3190	-.7630
1490	49	27	.2580	.6767	-.6896
1500	51	28	-.6436	.2943	-.7065
1510	52	29	.3183	.6958	-.6439
1520	54	30	-.7150	.2708	-.6446
1530	58	31	-.1771	.6284	-.7574
1540	60	32	-.5153	.4086	-.7533

(S, C OR RETURN) >

123456789 123456789 123456789 123456789 123456789 123456789 123456789 123456789 123456789 123456789

1550	61	33	-.0481	.6613	-.7486
1560	63	34	-.6112	.3828	-.6927
1570	64	35	.0468	.6855	-.7265
1580	66	36	-.6909	.3588	-.6276
1590	67	37	.1239	.7057	-.6976
1600	69	38	-.7585	.3360	-.5584
1610	70	39	.1887	.7233	-.6643
1620	72	40	-.8157	.3141	-.4859
1630	76	41	-.2984	.6649	-.6848
1640	78	42	-.6517	.4435	-.6153
1650	79	43	-.1779	.6943	-.6974
1660	81	44	-.7286	.4209	-.5404
1670	82	45	-.0850	.7163	-.6926
1680	84	46	-.7911	.3994	-.4633
1690	85	47	-.0073	.7347	-.6784
1700	87	48	-.8419	.3787	-.3844
1710	88	49	.0598	.7506	-.6580
1720	90	50	-.8826	.3587	-.3040

1730

1740

(S,C OR RETURN)>

123456789 123456789 123456789 123456789 123456789 123456789 123456789 123456789 1234
56789

1750

1760

1770

1780

1790

1800

1810

1820

1830

1840

1850

1860

1870

1880

1890

1900

1910

1920

1930

1940

(S,C OR RETURN)>

123456789 123456789 123456789 123456789 123456789 123456789 123456789 1234
56789

1950

1960

1970

1980

1990

2000

2010

2020

2030

2040

2050

2060

2070

2080

2090

2100

2110

2120

2130

2140

(S,C OR RETURN)>

123456789 123456789 123456789 123456789 123456789 123456789 123456789 123456789 123456789 123456789

2150
2160
2170
2180
2190
2200
2210
2220
2230
2240
2250 0
2260 EOI
>

APPENDIX B

DEFLECTION AND SLOPE AT POINT B

Referring to Fig. 2-7, one obtains the reaction force at c from $\sum (M_z)_C = 0$:

$$R_C = \frac{M_0 - P(d - L)}{d - c} \quad (B.1)$$

where $(M_z)_C$ is the moment about z axis through point C.

To obtain the deflection and slope at B, the beam is divide into 2 portions.

(1) $c < x < d$

Considering the equilibrium of the portion of the beam to the right of point C (Fig. B-1), one can obtain

$$M_1 = (P + R_C)x - PL - R_C c - M_0 \quad (B.2)$$

The moment of inertia of the cross sectional area with respect to the neutral axis is

$$I_1 = \frac{\pi(r_s^4 - r_i^4)}{4} \quad (B.3)$$

Let E be the modulus of elasticity, the differential equation of the elastic line for the beam is

$$\begin{aligned}
 y'' &= -\frac{M_1}{EI_1} \\
 &= -\frac{[(P + R_C)x - (PL + R_Cc + M_0)]}{EI_1}
 \end{aligned} \tag{B.4}$$

Let

$$A_1 = -\frac{(P + R_C)}{EI_1} \tag{B.5}$$

$$A_2 = \frac{(PL + R_Cc + M_0)}{EI_1} \tag{B.6}$$

Then

$$y'' = A_1 x + A_2 \tag{B.7}$$

Separating variables and integrating twice one obtains

$$y = \frac{A_1}{6}x^3 + \frac{A_2}{2}x^2 + c_1x + c_2 \tag{B.8}$$

where c_1 and c_2 are constants of integration.

The integration constants are determined from the conditions:

$$y = 0 \text{ at } x = c \text{ and } x = d$$

Substituting these conditions into the equation (B.8), one obtains

$$c_1 = -\frac{1}{6}[A_1(c^2 + cd + d^2) + 3A_2(c + d)] \quad (B.9)$$

$$c_2 = \frac{cd}{6}[A_1(c + d) + 3A_2] \quad (B.10)$$

With these values, the slope at $x = c$ can be obtained

$$y_C' = \frac{c}{2}(A_1c + 2A_2) + c_1 \quad (B.11)$$

(2) $b < x < c$

Fig. B-2 is a free body diagram of the portion of the beam to the right of point B. One obtains

$$M_2 = P(x - L) - M_0 \quad (B.12)$$

$$I_2 = I_1 = \frac{\pi(r_s^4 - r_i^4)}{4}$$

The differential equation is

$$\begin{aligned} y'' &= -\frac{M_2}{EI_1} \\ &= \frac{-Px + (PL + M_0)}{EI_1} \end{aligned} \quad (B.13)$$

Let

$$A_3 = -\frac{P}{EI_1} \quad (B.14)$$

$$A_4 = \frac{PL + M_0}{EI_1} \quad (B.15)$$

Then

$$y'' = A_3 x + A_4 \quad (B.16)$$

$$y' = \frac{A_3}{2}x^2 + A_4 x + C_3 \quad (B.17)$$

$$y = \frac{A_3}{6}x^3 + \frac{A_4}{2}x^2 + C_3 x + C_4 \quad (B.18)$$

$$\text{At } x = c, y = 0 \text{ and } y' = y'_C = \frac{c}{2}(A_1 c + 2A_2) + C_1,$$

one obtains

$$C_3 = y'_C - \frac{c}{2}(A_3 c + 2A_4) \quad (B.19)$$

$$C_4 = -\frac{c}{6}(A_3 c^2 + 3A_4 c + 6C_3) \quad (B.20)$$

Then the deflection and slope of point B can be obtained

$$y_B = \frac{b}{6}(A_3 b^2 + 3A_4 b + 6C_3) + C_4 \quad (B.21)$$

$$y'_B = \frac{b}{2}(A_3 b + 2A_4) + C_3 \quad (B.22)$$

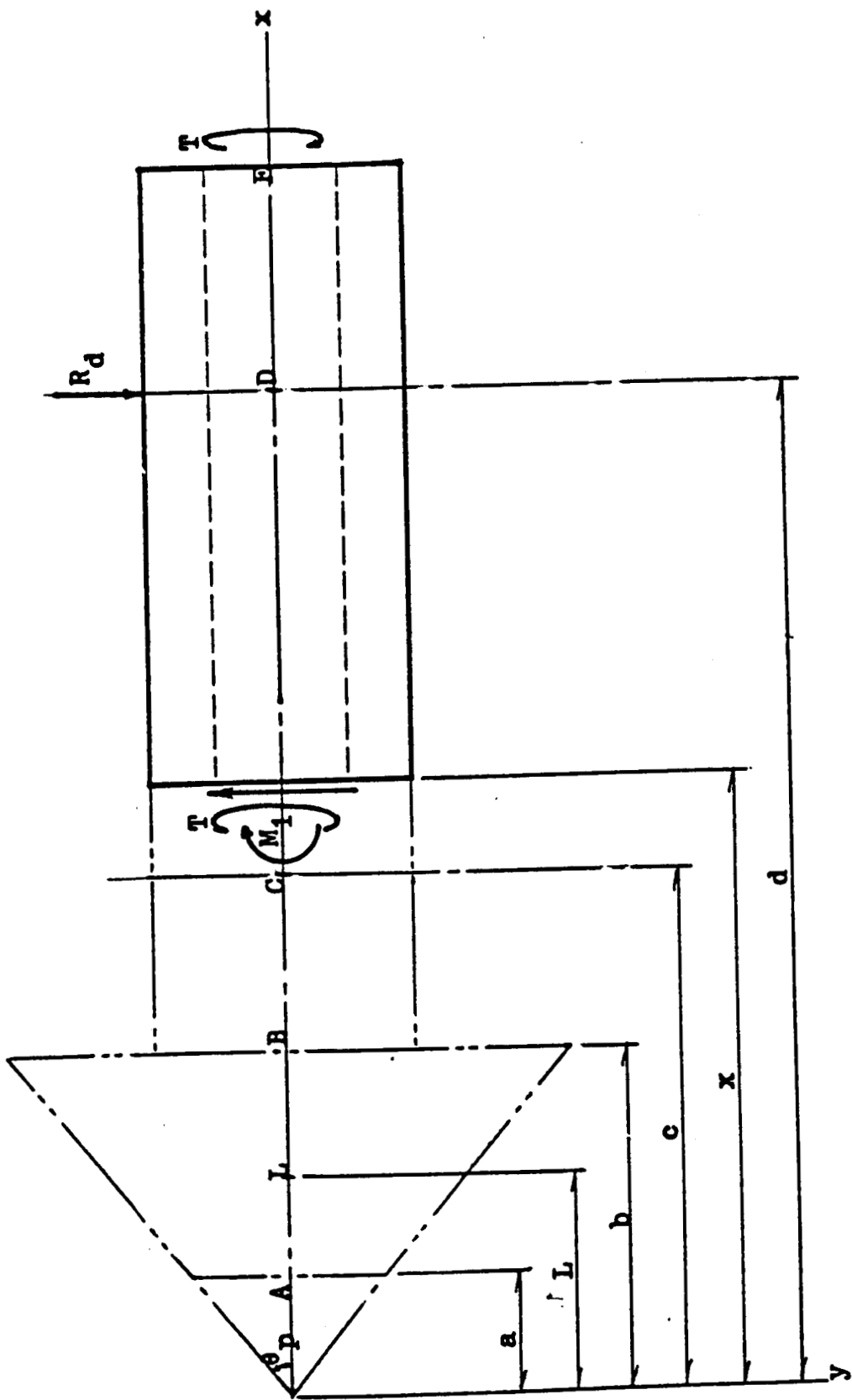


Fig. B-1 Free body diagram of the beam to the right of point C

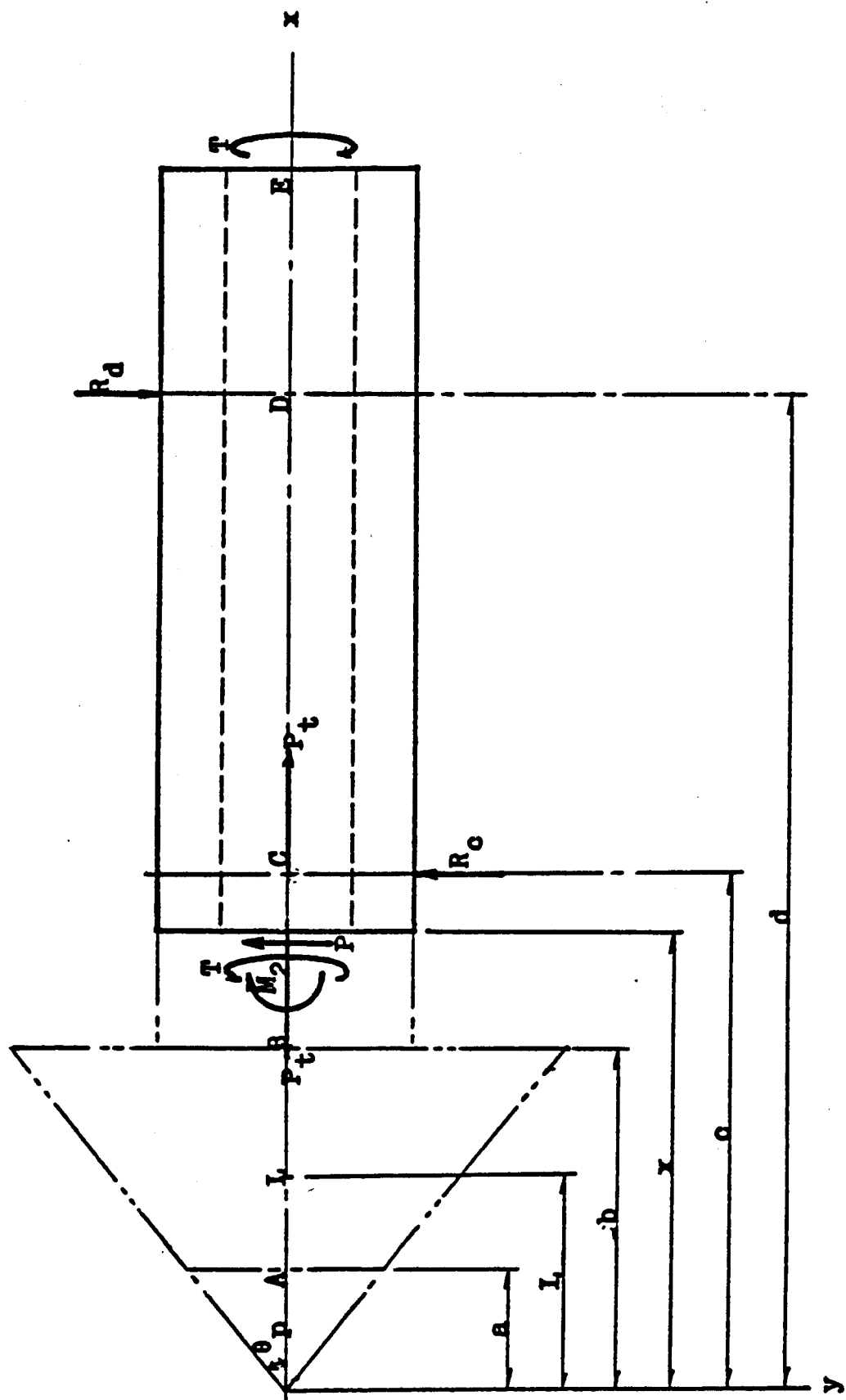


FIG. B-2 Free body diagram of the beam to the right of point B

1. Report No. NASA CR-179620 AVSCOM TR-B7-C-16	2. Government Accession No.	3. Recipient's Catalog No.	
4. Title and Subtitle A Simplified Computer Solution for the Flexibility Matrix of Contacting Teeth for Spiral Bevel Gears		5. Report Date June 1987	
7. Author(s) C.Y. Hsu and H.S. Cheng		6. Performing Organization Code	
9. Performing Organization Name and Address Northwestern University Evanston, Illinois 60201		8. Performing Organization Report No. None	
12. Sponsoring Agency Name and Address U.S. Army Aviation Research and Technology Activity - AVSCOM, Propulsion Directorate, Lewis Research Center, Cleveland, Ohio 44135 and NASA Lewis Research Center, Cleveland, Ohio 44135.		10. Work Unit No. TL161102AH45 505-63-51	
15. Supplementary Notes Project Manager, John J. Coy, Propulsion Directorate, U.S. Army Aviation Research and Technology Activity - AVSCOM, Lewis Research Center.		11. Contract or Grant No. NSG-3143	
16. Abstract A simplified analysis for obtaining the flexibility matrix of the contacting teeth of a pair of spiral bevel gears is presented. An existing finite element code SAP IV was used for computing the tooth deformation. The total deformation is obtained by superimposing the tooth deformation on the shaft deformation which was obtained from conventional beam theory. This simplified analysis was incorporated in the main computer code developed earlier by Chao (NASA CR-4077) for computing dynamic loads in spiral bevel gears.		13. Type of Report and Period Covered Contractor Report Final	
17. Key Words (Suggested by Author(s)) Gears; Transmissions; Machine design; Vibration		18. Distribution Statement Unclassified - unlimited STAR Category 37	
19. Security Classif. (of this report) Unclassified	20. Security Classif. (of this page) Unclassified	21. No. of pages 72	22. Price* A04